The study of accelerating DE models in Saez–Ballester theory of gravitation

T. Vinutha[a] , K. Venkata Vasavi[b]

Department of Applied Mathematics, Andhra University, Visakhapatnam 530003, India

Abstract The investigation in the present work is carried out on the spatially homogeneous and anisotropic axially symmetric space-time in the presence of two fluids, one being the pressureless matter and other being the different kinds of holographic dark energy (HDE). Eventually, in the present work, cosmological models with Tsallis HDE, Renyi HDE, Sharma–Mittal HDE by taking Hubble radius as infrared (IR) cutoff ($L = H^{-1}$) are obtained. The geometrical and matter parts of space-time are solved within the Saez–Ballester scalar-tensor theory of gravitation. Interestingly, in this study a time varying deceleration parameter (q) which exhibits a transition from deceleration to acceleration phase is obtained without assuming any scale factor. In the present work, the study of cosmic expansion is done through the scalar field (ϕ) and various cosmological parameters like EoS, deceleration, statefinder, etc. The EoS parameter exhibits quintom-like behavior for Tsallis HDE model, the transition from matter-dominated phase to phantom phase for Renyi HDE model, whereas it shows quintessence behavior for Sharma–Mittal HDE. The stability analysis for three models is studied through the squared speed of sound (v_s^2). For all redshift (z) values $v_s^2 > 0$, the Sharma–Mittal HDE model is stable throughout the universe's expansion. In this work, the obtained results match with recent observational data.

1 Introduction

At present, the universe is going through a phase of accelerated expansion, and this is suggested by numerous observational data such as type Ia supernovae [1–4], cosmic microwave background (CMB) anisotropies [5–7], large-scale structure (LSS) [8–11]. This expanding phase of cosmos is due to some mysterious force containing repulsive gravitational effects, referred as dark energy (DE). This exotic type of fluid consists of positive energy density and negative pressure. There are mainly two ways to study this mysterious force and cosmic acceleration. To understand this strange component, the first approach is a modification in the geometric part of the action principle in general relativity (GR), resulting in alternative theories of gravity. The modification in geometric parts involves some invariants depending on specific features like scalars, torsion, curvature, etc. The different alternative theories of gravity are scalar-tensor theories like Brans–Dicke theory [12], Saez–Ballester theory [13] and modified theories of gravity like $f(R)$ [14–16], $f(T)$ [17–19], $f(R, T)$ [20] and so on. Another approach is by modifying the matter part of Einstein field equations, which leads to various dynamical DE models. Besides these various dynamical DE models, the cosmological constant(Λ) is the simplest fundamental candidate, but this cosmological constant experiences enormous incidents and fine-tuning problems [21, 22]. Due to this reason, various dynamical DE models have been proposed like ghost [23], K-essence [24, 25], quintessence [26], phantom [27, 28], Chaplygin gas [29–31], tachyon [84], polytropic gas [33, 34], holographic dark energy models (HDE) [35–39].

The holographic dark energy (HDE) has become an interesting concept in present period as it has some significant features regarding quantum gravity [35, 40, 41], so it has been proposed as candidate of dark energy (DE) to explain the recent phase transition of cosmos. The HDE is based on holographic principle (HP) [40], which is originated from the thermodynamics of the blackhole. The holographic principle is even applied to string theory by Susskind [41]. This principle proposes that the degrees of freedom of entropy of a system depends on its bounding area but not on its volume. The formation of blackholes gives a limit as it gives a relation between ultraviolet cutoff (short-distance cutoff Λ) and the infrared cutoff (long-distance cutoff L). The energy density related to HDE [42] is given as

$$\rho_{de} = 3c^2 m_p^2 L^{-2},$$

in the above equation, the reduced Planck mass and infrared (IR) cut-off were denoted as m_p, L, respectively, and the numerical parameter as c. The HDE is inversely proportional to the square of infrared cutoff, so due to this fact, the horizon is taken in the

[a] e-mail: vinuthatummala@gmail.com (corresponding author)

[b] e-mail: venkatavasavi3@gmail.com

form of Hubble horizon (H^{-1}), event horizon, particle horizon, conformal universe age, Ricci scalar radius, Grand-Oliveros cutoff. Hence, horizon entropy is treated as the backbone of HDE.

Li [35] has shown that Hubble horizons and particle horizons are not in good agreement with the cosmos while the future event horizon is the best model for non-interacting holographic DE with suitable constant c. The Hubble horizon is a natural candidate for IR cut-off which is also free from causality, but Hsu [43] found that it gives wrong equation of state (EoS) of DE. Later on, it was shown [36] that if there is an interaction between two dark components of the cosmos the identification of L with Hubble horizon, $L = H^{-1}$, may give suitable EoS of DE. It has also been shown that it necessarily implies a constant ratio of the energy densities of the two components regardless of the details of the interaction. Thus, the HDE models may also alleviate the cosmic coincidence problem which provides an advantage to HDE models over the other DE models. These HDE models with various infrared cutoffs prove that the value of transition redshift from early deceleration phase ($q > 0$) to current acceleration phase ($q < 0$) is in agreement with modern observational [44–51]. Shanthi and Sobhan babu [52, 53] have investigated the Tsallis holographic dark energy (considering IR cut-off as Hubble radius, i.e., $L = H^{-1}$) in homogeneous and anisotropic Kantowski–Sachs and Bianchi type-III cosmological models within the frame-work of Saez–Ballester scalar tensor theory of gravitation

As gravity is a long-range interaction, generalized statistical mechanics can be used to investigate gravitational systems. According to this, the Bekenstein entropy can be determined by applying Tsallis statistics to the system [54–56]. Based on this recently, three new HDE models have been proposed, titled Tsallis holographic dark energy (THDE) [57, 58], Renyi holographic dark energy (RHDE) [59] and Sharma–Mittal holographic dark energy (SMHDE) [60]. The late-time accelerated universe can be described by these three models with Bekenstein entropy. In non-interacting universe, Tsallis HDE is never stable [57, 58] at the classical level, Renyi HDE shows more stability by itself [59], Sharma HDE is stable at the classical level [60]. Aditya et al. [61] worked on Tsallis HDE in logarithmic Brans–Dicke theory using flat FRW universe. Aditya and Prasanthi [62, 63] worked on the Renyi HDE model in general relativity using Bianchi-VI_0 and Kantowski–Sachs space-time.

Several authors worked on these three newly proposed HDE models using different theories in a flat FRW universe. A few of them are Younas et al. [64], who have studied Tsallis, Renyi, Sharma–Mittal entropies in flat FRW universe using Chern–Simons gravity. Maity and Debnath [65] worked on D-dimensional fractal universe discussing these three HDE models. Iqbal and Jawad [66] studied these three HDE models in a flat FRW universe within the frame of DGP braneworld. Jawad et al. [67] have investigated Tsallis, Renyi, Sharma–Mittal HDE models in loop quantum cosmology. All these works are carried on homogeneous and isotropic FRW universe. The observations from CMBR [68] have revealed the existence of transition from the anisotropic phase of the universe to the isotropic phase. So to represent the early phase of cosmos, only the isotropic model cannot express the early stage of cosmos; to overcome this, it is always suggestible to study anisotropic and spatially homogeneous space-time [69]. So due to this cause, the interest in anisotropic and spatially homogeneous space-times has been increased over the last few decades in theoretical cosmology. With these exciting aspects in the present-day universe, we consider spatially homogeneous and anisotropic axially symmetric space-time in the present paper.

As Einstein's theory of general relativity does not seem to resolve some of the important problems in cosmology such as dark matter or the missing matter problem there has been considerable interest in alternative theories of gravitation. The most important among them are scalar-tensor theories proposed by Brans–Dicke, Saez–Ballester and so on. The Saez–Ballester scalar-tensor theory of gravitation was developed by Saez and Ballester [13] in 1986. In this scalar-tensor theory, the metric potentials are coupled with dimensionless scalar field ϕ. Here, the dimensionless coupling constant w governs the strength of coupling between gravity and field further the missing matter problem in non-flat FRW cosmologies can be solved using this theory.

The action principle for this scalar-tensor theory is expressed as

$$A = \int_R (L + \chi L_m)\sqrt{-g}\, dx^1 dx^2 dx^3 dx^4,$$

With a slight variation to this A (action principle) so that the metric and scalar field vanishes at the boundary region R. Hence, the action principle gives rise to field equations of this scalar-tensor theory as

$$R_{ij} - \frac{1}{2}R g_{ij} - w\phi^n\left(\phi_{,i}\phi_{,j} - \frac{1}{2}g_{ij}\phi_{,k}\phi^{,k}\right) = -8\pi G T_{ij}, \tag{1}$$

In the above equation (1), w is the dimensionless constant, T_{ij} is energy momentum tensor, n is the arbitrary dimensionless constant, G is gravitational constant ($8\pi G = 1$) and ϕ is the scalar field satisfying the following equation

$$2\phi^n \phi_{;i}^{;i} + n\phi^{n-1}\phi_{,k}\phi^{,k} = 0, \tag{2}$$

here, in equation (2) the partial and covariant differentiation are denoted by comma (,) and semi-colon (;), respectively. The energy conservation equation is given by

$$T_{;j}^{ij} = 0 \tag{3}$$

Many researchers like Ramesh et al. [70], Rao et al. [71], Rasouli et al. [72], Sharma et al. [73], have worked with different cosmological models using this scalar-tensor theory. Mishra et al. [74–76] worked on this theory using time-varying deceleration parameter (DP), cosmological and gravitational constants (Λ, G) and bilinear varying deceleration parameter (DP). Rasouli et al.

[77] have discussed the cosmic acceleration for the future time by considering two scalar fields, the first scalar representing the Saez–Ballester theory and the second one having an extra dimension. Also, few works can be found in [78–83].

The HDE model is the first theoretical model of DE inspired by the HP, and it agrees well with current cosmological evidence. As a result, HDE is a really attractive option for DE. Moreover, the HDE hypothesis has received a lot of interest and has been intensively investigated in the last few years. These are as follows

1. The features of HDE are addressed in several modified gravity theories, including the scalar-tensor theories like Brans–Dicke theory, Saez–Ballester theory, and DGP brane-world theories, which can be found in the works [71, 84–87].

2. The HDE is employed in the reconstruction of various scalar-field DE and modified gravity models.

The Saez–Ballester theory provides a dynamical framework that is more suitable to study HDE models as HDE belongs to the family of dynamical DE candidates. Setare [84] discussed the holographic dark energy model in the Brans–Dicke theory. The cosmological dynamics of the interacting holographic dark energy model are obtained by Setare and Vanegas [88]. Aditya and Reddy discussed FRW type kaluza–klein modified holographic Ricci dark energy models in Brans–Dicke theory of gravitation [89].

Hence, by the motivation of these works we have discussed Tsallis, Renyi, Sharma–Mittal HDE models in axially symmetric space-time using Saez–Ballester scalar-tensor theory of gravitation in the present work. The plan of this paper is as follows metric, and its field equations are discussed in Sect. 2, and the solutions of the field equations are obtained in Sect. 3. The behavior of cosmological parameters along with graphical representation is discussed in Sect. 4, and finally, the conclusions are discussed in Sect. 5.

2 Metric and field equations

The homogeneous and anisotropic axially symmetric space-time proposed by Bhattacharaya and Karade [90] is given by

$$ds^2 = dt^2 - A^2(t)\big[d\chi^2 + f^2(\chi)d\phi^2\big] - B^2(t)dz^2, \tag{4}$$

where χ, ϕ, z are comoving coordinates, A, B are functions of cosmic time t and f is a function of coordinate χ alone.

The Saez–Ballester field equations for combined matter and dark energy (DE) are given as

$$R_{ij} - \frac{1}{2}Rg_{ij} - w\phi^n\left(\phi_{,i}\phi_{,j} - \frac{1}{2}g_{ij}\phi_{,k}\phi^{,k}\right) = -(T_{ij} + \overline{T}_{ij}) \tag{5}$$

The conservation equation for energy momentum tensor is given by

$$\left(T_{ij} + \overline{T}_{ij}\right)_{;j} = 0 \tag{6}$$

In equation (5), T_{ij} is energy momentum tensor for pressureless matter and $\overline{T}_{ij}$ is HDE which are given as

$$T_{ij} = \rho_m u_i u_j \tag{7}$$

$$\overline{T}_{ij} = (\rho_{de} + p_{de})u_i u_j - p_{de}g_{ij} \tag{8}$$

where ρ_m is energy density of matter, p_{de} and ρ_{de} are the pressure and energy density of HDE, respectively, u_i is the four-velocity vector component of fluid satisfying $u_i = (0, 0, 0, 1)$. As the equation of state (EoS) parameter is defined as $\omega_{de} = \frac{p_{de}}{\rho_{de}}$, equations (7) and (8) become

$$T_{ij} = diag[0, 0, 0, \rho_m] \tag{9}$$

$$\overline{T}_{ij} = diag[-\omega_{de}\rho_{de}, -\omega_{de}\rho_{de}, -\omega_{de}\rho_{de}, \rho_{de}]$$

and after parametrization it reduces to

$$\overline{T}_{ij} = diag\big[-\omega_{de}\rho_{de}, -\omega_{de}\rho_{de}, -(\omega_{de} + \gamma)\rho_{de}, \rho_{de}\big] \tag{10}$$

here, the skewness parameter γ is the deviation from EoS parameter (ω_{de}) on z-direction.

The field equations (5), (2) for the metric (4) are as follows

$$\frac{\ddot{A}}{A} + \frac{\dot{A}\dot{B}}{AB} + \frac{\ddot{B}}{B} - \frac{w\phi^n\dot{\phi}^2}{2} = -\omega_{de}\rho_{de} \tag{11}$$

$$\frac{\dot{A}^2}{A^2} + \frac{2\ddot{A}}{A} - \frac{f''}{A^2 f} - \frac{w\phi^n\dot{\phi}^2}{2} = -\omega_{de}\rho_{de} - \gamma\rho_{de} \tag{12}$$

$$\frac{\dot{A}^2}{A^2} + \frac{2\dot{A}\dot{B}}{AB} - \frac{f''}{A^2 f} + \frac{w\phi^n\dot{\phi}^2}{2} = \rho_{de} + \rho_m \tag{13}$$

$$\ddot{\phi} + \dot{\phi}\left(\frac{2\dot{A}}{A} + \frac{\dot{B}}{B}\right) + \frac{n\dot{\phi}^2}{2\phi} = 0 \tag{14}$$

The functional dependence of the given line element with the help of (12) and (13) gives the relation

$$\frac{f''}{f} = k_1^2, k_1^2 = const \tag{15}$$

If $k_1 = 0$, then

$$f(\chi) = (const)\chi, \; 0 < lt; \chi < lt; \infty$$

For suitable choice of units for ϕ, the constant can be equal to unity. This leads to $f(\chi) = \chi$ resulting in a flat model of the universe [91].

3 Solutions of field equations

With the help of equation (15), equations (11)-(14) reduce to

$$\frac{\ddot{A}}{A} + \frac{\dot{A}\dot{B}}{AB} + \frac{\ddot{B}}{B} - \frac{w\phi^n\dot{\phi}^2}{2} = -\omega_{de}\rho_{de} \tag{16}$$

$$\frac{\dot{A}^2}{A^2} + \frac{2\ddot{A}}{A} - \frac{w\phi^n\dot{\phi}^2}{2} = -\omega_{de}\rho_{de} - \gamma\rho_{de} \tag{17}$$

$$\frac{\dot{A}^2}{A^2} + \frac{2\dot{A}\dot{B}}{AB} + \frac{w\phi^n\dot{\phi}^2}{2} = \rho_{de} + \rho_m \tag{18}$$

$$\ddot{\phi} + \dot{\phi}\left(\frac{2\dot{A}}{A} + \frac{\dot{B}}{B}\right) + \frac{n\dot{\phi}^2}{2\phi} = 0 \tag{19}$$

The energy conservation equation $(T_{ij} + \overline{T}_{ij})_{;j} = 0$ is obtained as

$$\dot{\rho}_m + \dot{\rho}_{de} + (\rho_m + \rho_{de} + \rho_{de}\omega_{de})\left(\frac{2\dot{A}}{A} + \frac{\dot{B}}{B}\right) + \gamma\rho_{de}\frac{\dot{B}}{B} = 0 \tag{20}$$

Here, we assume there is no energy transfer between dark matter and dark energy, so the above equation reduces into two separate conservation equations as

$$\dot{\rho}_m + \rho_m\left(\frac{2\dot{A}}{A} + \frac{\dot{B}}{B}\right) = 0 \tag{21}$$

$$\dot{\rho}_{de} + (\rho_{de} + \rho_{de}\omega_{de})\left(\frac{2\dot{A}}{A} + \frac{\dot{B}}{B}\right) + \gamma\rho_{de}\frac{\dot{B}}{B} = 0 \tag{22}$$

The obtained four field equations (16)-(19) contain six unknowns namely A, B, ϕ, ω_{de}, ρ_m, γ, so in order to solve these unknowns we assume the following two physical valid conditions.

Here, we assume the power law relationship between metric potentials by using the condition $\sigma \propto \theta$ (shear scalar (σ), expansion scalar (θ)), which is considered as,

$$A = B^l \tag{23}$$

here, l is a positive constant that preserves the anisotropy of the model for $l \neq 1$ and for $l = 1$, the model leads to a isotropic model. The physical importance for considering this relation is given by Thorne [92], and from the velocity-redshift observations for extragalactic sources advice that Hubble expansion of cosmos is isotropic for present time with the range $\approx 33\%$ [93, 94]. These observations suggest that the cosmos attains isotropy for $\frac{\sigma}{H} \leq 0.3$. Further, the valid physical assumption was given by Collins [95] for the case of perfect fluids and barotropic EoS. Many authors have derived the solutions by using this condition few of them are Aditya et al. [62, 96], Mishra and Sahoo [97].

From equations (16), (17) and (23), we obtain

$$\frac{\ddot{B}}{B} + 2l\frac{\dot{B}}{B} = \frac{B}{\dot{B}}\frac{\gamma\rho_{de}}{(1-l)} \tag{24}$$

As in recent times, it has been a quite interesting part in finding the general and explicit solutions of the derived equations, so the skewness parameter is assumed in terms of energy density of dark energy (DE). The relation among skewness parameter (γ) and energy density of DE (ρ_{de}) was considered by Akarsu et al. [98], in the process of solving anisotropic DE models with LRS Bianchi type-I universe. Now, in order to solve equation (24) we consider a relationship between skewness parameter (γ) and energy density (ρ_{de}) of DE as

$$\gamma = \frac{\dot{B}}{B} \frac{(1-l)\gamma_1}{\rho_{de}}, \tag{25}$$

where γ_1 is an arbitrary constant. Various authors have worked with this assumption [99, 100]; alternatively, in the literatures [96, 101] the authors have studied this assumption in the study of anisotropic DE models in various theories of gravitation. Now, on solving equation (24) with the help of (25), we obtain the metric coefficients

$$A = \left(c_1(2l+1)\frac{exp(\gamma_1 t)}{\gamma_1} + c_2(2l+1) \right)^{\frac{l}{(2l+1)}} \tag{26}$$

$$B = \left(c_1(2l+1)\frac{exp(\gamma_1 t)}{\gamma_1} + c_2(2l+1) \right)^{\frac{1}{(2l+1)}} \tag{27}$$

and using the values of A, B in (19) we obtain Saez–Ballester scalar field ϕ as

$$\phi = \left(\frac{2+n}{2} \right)^{\frac{2}{2+n}} \left(\frac{\gamma_1 c_3 t - c_3 log(c_1 exp(\gamma_1 t) + \gamma_1 c_2)}{\gamma_1 c_2 + 2\gamma_1 c_2 l} \right)^{\frac{2}{2+n}} \tag{28}$$

In above equations (26), (27), (28), c_1, c_2, c_3 are integrating constants and by substituting the values of A, B in (4) the line-element becomes

$$ds^2 = dt^2 - \left(c_1(2l+1)\frac{exp(\gamma_1 t)}{\gamma_1} + c_2(2l+1) \right)^{\frac{2l}{(2l+1)}} \left[d\chi^2 + f^2(\chi)d\phi^2 \right]$$
$$- \left(c_1(2l+1)\frac{exp(\gamma_1 t)}{\gamma_1} + c_2(2l+1) \right)^{\frac{2}{(2l+1)}} dz^2$$

4 Tsallis holographic dark energy

The energy density (ρ_{de}) for Tsallis HDE [57] is defined as

$$\rho_{de} = \alpha L^{2\delta - 4} \tag{29}$$

where α is a unknown parameter, L is infrared (IR) cutoff. Here, we assume Hubble horizon as IR cutoff, so we have $L = H^{-1}$. From this, energy density of THDE becomes

$$\rho_{de} = \alpha H^{4-2\delta} \tag{30}$$

H is the Hubble parameter and its value for the present model is obtained as

$$H = \frac{1}{3}\left(\frac{2\dot{A}}{A} + \frac{\dot{B}}{B} \right) = \frac{c_1 \gamma_1 exp(\gamma_1 t)}{(3c_1 exp(\gamma_1 t) + 3c_2 \gamma_1)} \tag{31}$$

By substituting equation (31) in (30), we obtain the energy density (ρ_{de}) for Tsallis HDE as

$$\rho_{de} = \frac{\alpha 9^\delta c_1^4 \gamma_1^4 exp(4\gamma_1 t)(\frac{c_1 \gamma_1 exp(\gamma_1 t)}{(c_1 exp(\gamma_1 t)+c_2 \gamma_1)})^{-2\delta}}{81(c_1 exp(\gamma_1 t) + c_2 \gamma_1)^4} \tag{32}$$

Now, from equations (18), (25) with the help of equation (32) we obtain the values of ρ_m, γ

$$\left. \begin{array}{l} \rho_m = \frac{-1}{81(l+\frac{1}{2})^2(c_1 exp(\gamma_1 t)+c_2 \gamma_1)^4}\left(\gamma_1^2\left(c_1^4 exp(4\gamma_1 t)\left(\alpha \gamma_1^2 9^\delta(l+\frac{1}{2})^2(\frac{c_1 \gamma_1 exp(\gamma_1 t)}{(c_1 exp(\gamma_1 t)+c_2 \gamma_1)})^{(-2\delta)} - \frac{81l^2}{4} - \frac{81l}{2} \right) \right.\right. \\ \left.\left. - \frac{81c_1^2(c_2^2 l(l+2)\gamma_1^2 + \frac{wc_3^2}{2})exp(2\gamma_1 t)}{4} - \frac{81c_2 \gamma_1(c_1^3 l(l+2)exp(3\gamma_1 t) + \frac{wc_3^2(c_1 exp(\gamma_1 t)+\frac{c_2 \gamma_1}{2})}{2})}{2} \right)\right) \end{array} \right\} \tag{33}$$

$$\gamma = -\frac{819^{-\delta}(-1+l)exp(-3\gamma_1 t)(c_1 exp(\gamma_1 t)+c_2 \gamma_1)^3(\frac{c_1 \gamma_1 exp(\gamma_1 t)}{(c_1 exp(\gamma_1 t)+c_2 \gamma_1)})^{2\delta}}{\alpha \gamma_1^2 c_1^3(2l+1)} \tag{34}$$

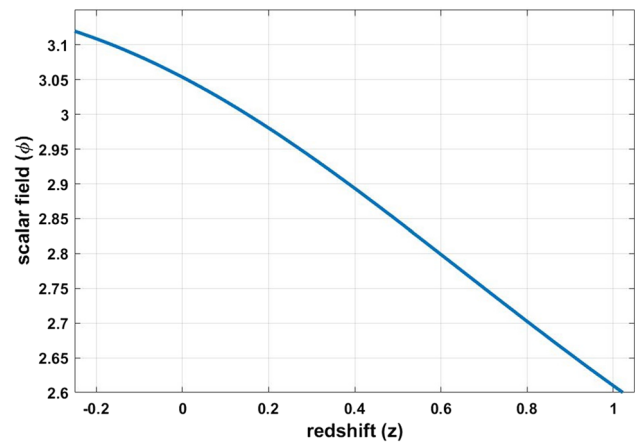**Fig. 1** Plot of scalar field (ϕ) versus redshift (z) for $n = 0.01, l = 0.325, \gamma_1 = 0.12$

Fig. 2 Plot of energy density (ρ_{de}) versus redshift (z) for THDE model
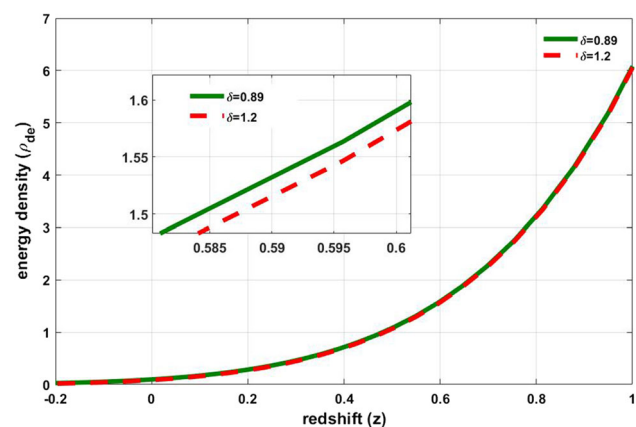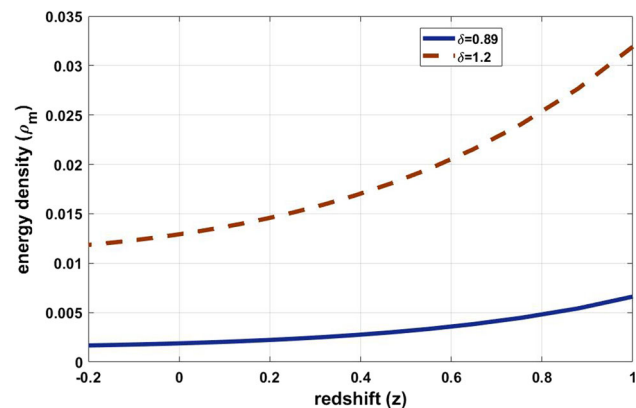

**Fig. 3** Plot of energy density of matter (ρ_m) versus redshift (z)

In order to study the behavior of energy densities ρ_m, ρ_{de}, skewness parameter (γ) of Tsallis, Renyi, Sharma–Mittal HDE models, we plot them (ρ_m, ρ_{de}, γ) with respect to redshift (z) (redshift is defined as $1 + z = \frac{a_0}{a(t)}$; we assume $a_0 = 1$).

From Fig. 1, it is observed that the scalar field (ϕ) is positive throughout the evolution of cosmos and increases as redshift (z) decreases. The plots of energy density (ρ_{de}) of THDE and energy density for pressureless matter with respect to redshift (z) for two different values of $\delta = 0.89, 1.2$ are given in Figs. 2, 3. It is observed that for both the values of δ the energy density (ρ_{de}) of THDE and pressureless matter (ρ_m) are positive throughout the evolution of cosmos and decreases as redshift (z) decreases.

The skewness parameter (γ) corresponding to redshift (z) for $\delta = 0.89, 1.2$ is shown in Fig. 4. For both the values of δ, the skewness parameter is positive throughout the evolution of cosmos and increases as redshift (z) decreases.

Fig. 4 Plot of skewness parameter
(γ) versus redshift (z)
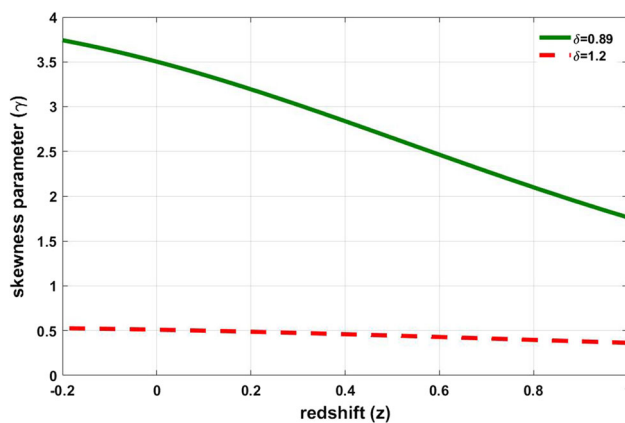
5 Renyi holographic dark energy

The energy density for Renyi HDE [59] is defined as

$$\rho_{de} = \frac{3c^2}{8\pi L^2(1 + \delta\pi L^2)},$$ (35)

where c, δ are constants, and IR cutoff is considered as Hubble radius (i. e. $L = H^{-1}$). Hence, the energy density for Renyi HDE is given as

$$\rho_{de} = \frac{3c^2 H^2}{8\pi\left(1 + \frac{\delta\pi}{H^2}\right)}$$ (36)

Now, using equation (31) in (36), we obtain the energy density (ρ_{de}) for Renyi HDE as

$$\rho_{de} = \frac{c^2 c_1^4 \gamma_1^4 exp(4\gamma_1 t)}{24\pi(c_1 exp(\gamma_1 t) + c_2\gamma_1)^2(18\pi c_2\gamma_1\delta c_1 exp(\gamma_1 t) + 9c_2^2\gamma_1^2\delta + 9c_1^2 exp(2\gamma_1 t)\pi\delta + c_1^2 exp(2\gamma_1 t)\gamma_1^2)}$$ (37)

From equations (18) and (25) with the help of (37) we obtain the expressions for ρ_m, γ as

$$\rho_m = \frac{\iota_1}{\iota_2}$$ (38)

$$\left.\begin{array}{l} \gamma = \dfrac{1}{c_1^3(2l+1)c^2\gamma_1^2} - 216\pi(-1+l)exp(-3\gamma_1 t)(c_1 exp(\gamma_1 t) + c_2\gamma_1)\left(c_1^2 exp(2\gamma_1 t)\left(\delta\pi + \dfrac{\gamma_1^2}{9}\right)\right) \\[4mm] \qquad + 2\gamma_1\delta\pi c_2(c_1 exp(\gamma_1 t) + \dfrac{c_2\gamma_1}{2})\Big) \end{array}\right\}$$ (39)

where

$$\iota_1 = -\gamma_1^2\left(c_1^4 exp(4\gamma_1 t)\left(\gamma_1^2(\pi(-6l^2 - 12l) + \left(l + \frac{1}{2}\right)^2 c^2) - 54\pi^2\delta l(l+2)\right) - 54\pi\left(c_1^2 exp(2\gamma_1 t)\left(\gamma_1^2\right.\right.\right.$$
$$\left(lc_2^2\delta(l+2)\pi + \frac{wc_3^2}{18}\right) + \frac{w\pi c_3^2\delta}{2}\right) + \frac{\pi\delta\gamma_1 c_2(4c_1^3 l(l+2)exp(3\gamma_1 t) + wc_3^2(c_2\gamma_1 + 2c_1 exp(\gamma_1 t)))}{2}\Big)\Big)\Big)$$

$$\iota_2 = 24\pi\left(l + \frac{1}{2}\right)^2\left(c_1^2 exp(2\gamma_1 t)(9\pi\delta + \gamma_1^2) + 9\gamma_1\pi c_2\delta(c_2\gamma_1 + 2c_1 exp(\gamma_1 t))\right)(c_1 exp(\gamma_1 t) + c_2)^2$$

For RHDE model, the energy density (ρ_{de}), energy density of pressureless matter corresponding to redshift (z) is shown in Figs. 5, 6. It is observed that both ρ_{de}, ρ_m are positive throughout the evolution of cosmos and decreases as redshift (z) decreases for both the values of $\delta = 0.89, 1.2$. Similarly, the positive value of skewness parameter with respect to redshift (z) for $\delta = 0.89, 1.2$ is observed in Fig. 7.

Fig. 5 Plot of energy density
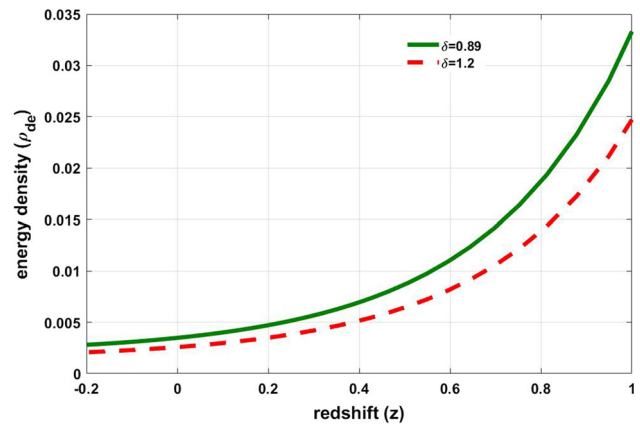(ρ_{de}) versus redshift (z) for
RHDE model

Fig. 6 Plot of energy density of
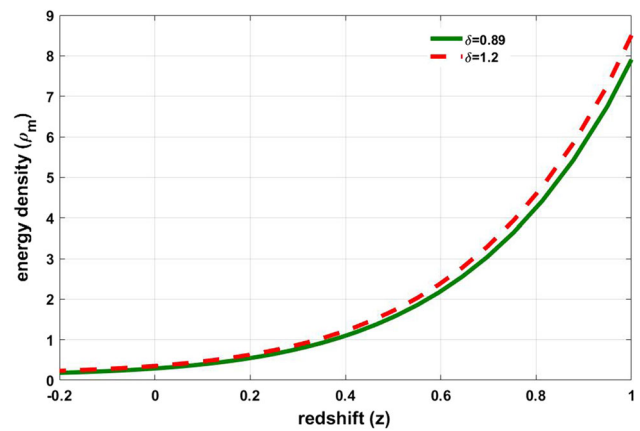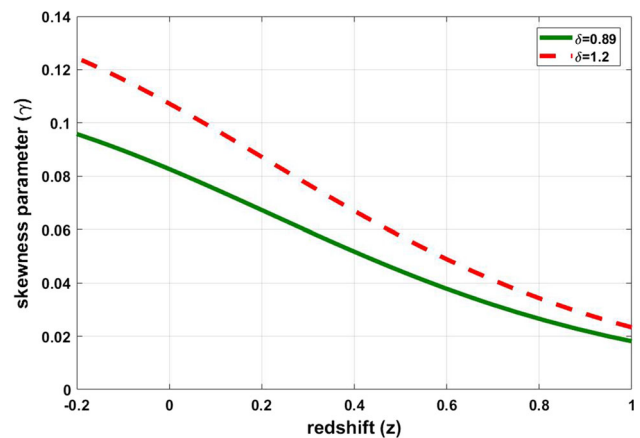matter (ρ_m) versus redshift (z)

Fig. 7 Plot of skewness parameter
(γ) versus redshift (z)

6 Sharma–Mittal holographic dark energy

The energy density (ρ_{de}) for Sharma–Mittal HDE [102] is defined as

$$\rho_{de} = \frac{3c^2\left((1 + \delta\pi L^2)^{\frac{R}{\delta}} - 1\right)}{8\pi R L^4} \tag{40}$$

where R, δ are two constants, L is the IR cutoff. By considering IR cutoff as Hubble horizon cutoff $L = H^{-1}$, the energy density
of Sharma–Mittal HDE becomes

$$\rho_{de} = \frac{3c^2 H^4\left((1 + \frac{\delta\pi}{H^2})^{\frac{R}{\delta}} - 1\right)}{8\pi R} \tag{41}$$

Fig. 8 Plot of energy density (ρ_{de}) versus redshift (z) for SHDE model
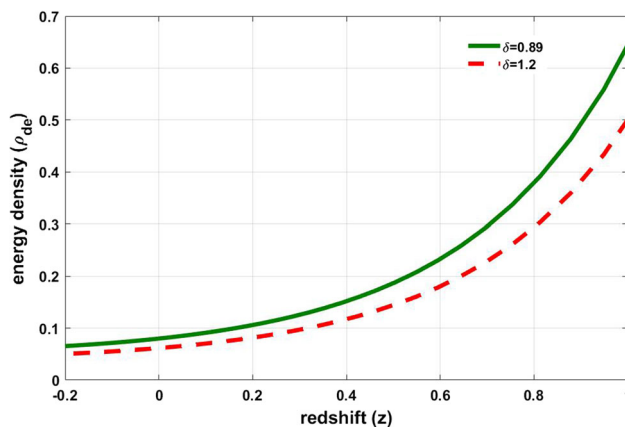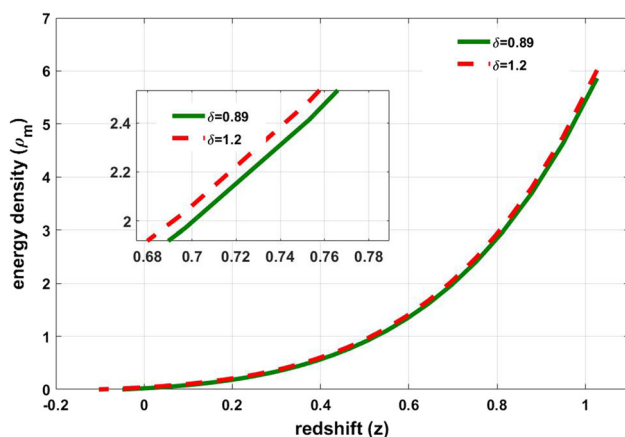

Fig. 9 Plot of energy density of matter (ρ_m) versus redshift (z)

By substituting equation (31) in (41), we obtain the energy density of Sharma–Mittal HDE as

$$\rho_{de} = \frac{c^2 c_1^4 \gamma_1^4 (\iota_7 - 1) exp(4\gamma_1 t)}{216(c_1 exp(\gamma_1 t) + c_2 \gamma_1)^4 \pi R} \tag{42}$$

Now, from Eqs. (18) and (25) with the help of (42) we obtain the expressions for ρ_m, γ as

$$\left.\begin{aligned}
\rho_m = \frac{-1}{216R\pi(l+\frac{1}{2})^2(c_1 exp(\gamma_1 t) + c_2\gamma_1)^4}\Bigg(& -54\left(c_2^2\gamma_1^2 l(l+2) + \frac{wc_3^2}{2}\right)Rc_1^2\pi exp(2\gamma_1 t) \\
+ c_1^4 exp(4\gamma_1 t)\left((\iota_7 - 1)\left(l+\frac{1}{2}\right)^2 c^2\gamma_1^2 - 54\pi Rl(l+2)\right) & - 27(4c_1^3 l(l+2)exp(3\gamma_1 t) \\
+ wc_3^2(c_2\gamma_1 + 2c_1 exp(\gamma_1 t)))c_2 R\pi\gamma_1\Bigg)\gamma_1^2 &
\end{aligned}\right\} \tag{43}$$

$$\left.\gamma = \frac{-216\pi R(-1+l)exp(-3\gamma_1 t)(c_1 exp(\gamma_1 t) + c_2\gamma_1)^3}{c^2\gamma_1^2 c_1^3(2l+1)(\iota_7 - 1)}\right\} \tag{44}$$

The energy density (ρ_{de}) of Sharma–Mittal HDE, energy density of pressureless matter for $\delta = 0.89, 1.2$ corresponding to redshift (z) are shown in Figs. 8, 9. From graphs, it can be observed that for both values of $\delta = 0.89, 1.2$ energy densities are positive throughout the evolution of cosmos and decreases as redshift (z) decreases. The skewness parameter with respect to redshift is shown in Fig. 10, and it is observed that it is positive throughout the evolution of cosmos and increases as redshift (z) decreases.

7 Cosmological parameters

Here, we discuss both physical and geometrical aspects such as volume (V), Hubble parameter (H), expansion scalar (θ), EoS parameter (ω_{de}), deceleration parameter (q), statefinder parameters $\{r, s\}$, squared speed of sound (v_s^2).

The average scale factor of the present model is obtained as

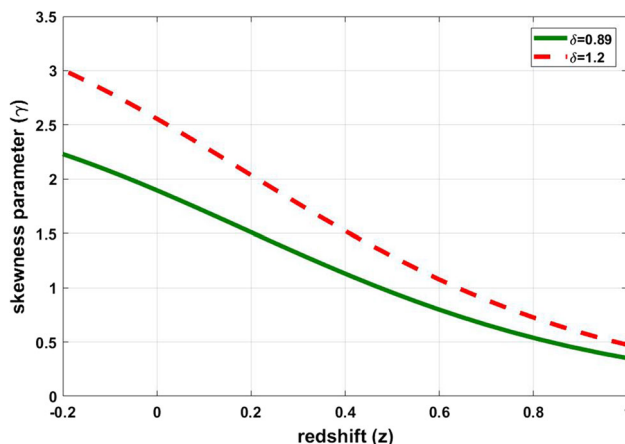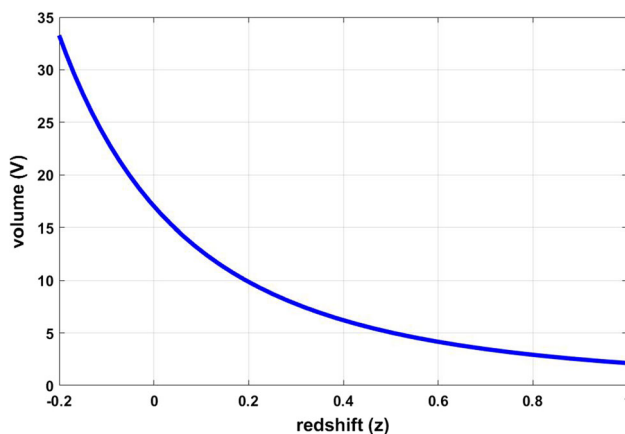**Fig. 10** Plot of skewness parameter (γ) versus redshift (z)

Fig. 11 Plot of volume (V) versus redshift (z)

$$a(t) = (A^2 B)^{\frac{1}{3}} = \left(\frac{(2l+1)(c_1 exp(\gamma_1 t) + c_2 \gamma_1)}{\gamma_1} \right)^{1/3}$$

The volume (V) of the present model is obtained as

$$V = \frac{(2l+1)(c_1 exp(\gamma_1 t) + c_2 \gamma_1)}{\gamma_1}$$

The volume (V) corresponding to redshift (z) is shown in Fig. 11. It is observed that volume is positive throughout the evolution of cosmos and increases as the redshift (z) decreases. These observations confirm the fact that the universe is expanding in an accelerating way, that is as the volume increases, the energy density decreases for the obtained model.

The Hubble parameter (H) of the present model is obtained as

$$H = \frac{c_1 \gamma_1 exp(\gamma_1 t)}{(3c_1 exp(\gamma_1 t) + 3c_2 \gamma_1)}$$

The expansion scalar for the present model is obtained as

$$\theta = 3H = \frac{c_1 \gamma_1 exp(\gamma_1 t)}{(c_1 exp(\gamma_1 t) + c_2 \gamma_1)}$$

8 EoS parameter

For Λ cold dark matter (CDM) model, the state of dark energy remains constant. For describing dark energy, an important model associated with it is equation of state (EoS) parameter, which is defined in terms of pressure (p_{de}) and energy density (ρ_{de}) and denoted as ω_{de}. Nowadays, to explain dark energy models, different equations of state (EoS) parameters came into existence, whose value needs not be a constant. Quintessence ($-1 < \omega_{de} < -\frac{-1}{3}$) model of dark energy, phantom model of dark energy ($\omega_{de} < -1$), vacuum era ($\omega_{de} = -1$) and quintom like behavior (combination of quintessence and phantom regions).

Fig. 12 Plot of EoS parameter (ω_{de}) of THDE versus redshift (z)
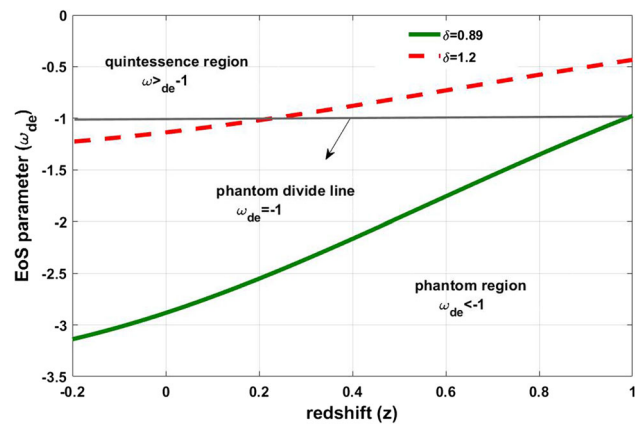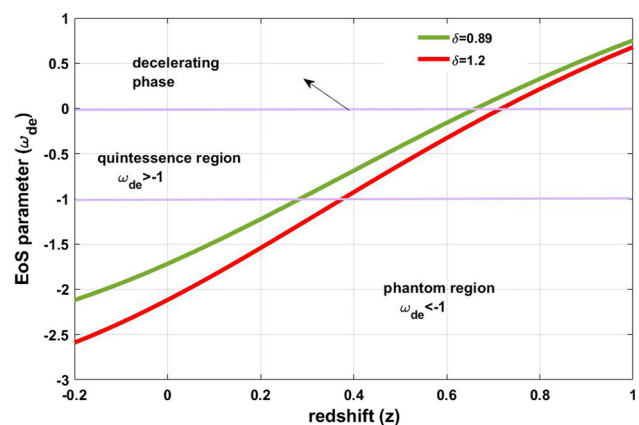

Fig. 13 Plot of EoS parameter (ω_{de}) of RHDE versus redshift (z)

The EoS parameter for Tsallis HDE model is obtained by solving equation (22), with the help of equations (26), (27), (32), (34).

$$\left.\begin{aligned}
\omega_{de} &= \frac{-1}{\alpha c_1^3 \gamma_1^2 (2l+1)^2 (c_1 exp(\gamma_1 t)+c_2\gamma_1)}(4exp(-\gamma_1 t)\\
&\left(\frac{-819^{-\delta}(-1+l)(3H)^{2\delta}exp(-2\gamma_1 t)(c_1 exp(\gamma_1 t)+c_2\gamma_1)^4}{4}\right.\\
&\left.+\alpha\left(\left(\left(exp(2\gamma_1 t)c_1^2 - 2(c_1\left(\delta-\frac{5}{2}\right)exp(\gamma_1 t)+c_2\gamma_1(-2+\delta)\right)\gamma_1 c_2\right)\left(l+\frac{1}{2}\right)^2 c_1^2\gamma_1^2\right)\right)
\end{aligned}\right\} \tag{45}$$

Similarly, the EoS parameter (ω_{de}) for Renyi, Sharma–Mittal HDE models is obtained by solving equation (22), with the help of equations (26), (27), (37), (39), (42), (44).

$$\omega_{de} = -1 - \iota_3 - \iota_4 \tag{46}$$

$$\omega_{de} = -1 - \iota_5 - \iota_6 \tag{47}$$

The values $\iota_3, \iota_4, \iota_5, \iota_6$ are given in the appendix section.

The EoS parameter (ω_{de}) for Tsallis, Renyi, Sharma–Mittal HDE models with respect to redshift (z) for two values of $\delta = 0.89, 1.2$ is shown in Figs. 12, 13, 14, respectively. From Fig. 12, it is observed that for $\delta = 0.89$ the ω_{de} exhibits phantom phase and for $\delta = 1.2$ the ω_{de} starts from quintessence phase and reaches to phantom phase crossing phantom divide line $(\omega_{de} = -1)$ (that is it shows quintom like behavior). The EoS parameter for Renyi HDE shows transition from decelerating phase to accelerating phase for both the values of $\delta = 0.89, 1.2$ at $z = 0.67$, $z = 0.72$, respectively. And the model starts from matter dominated phase and exhibits quintom like behavior for both the values of $\delta = 0.89, 1.2$ is shown in Fig. 13. The EoS parameter for Sharma–Mittal HDE for both the values of $\delta = 0.89, 1.2$ shows transition from decelerating phase to accelerating phase at $z = 0.475$, and model enters into quintessence phase from matter dominated phase is shown in Fig. 14.

Fig. 14 Plot of EoS parameter (ω_{de}) of SHDE versus redshift (z)
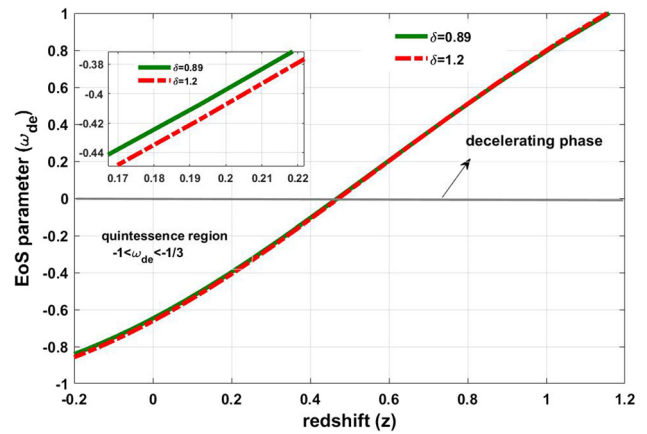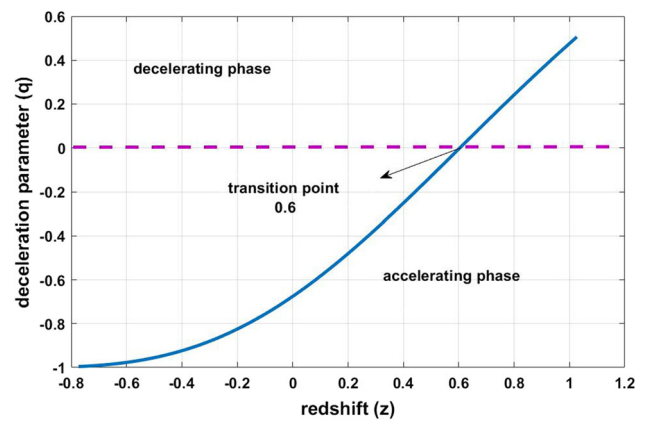

Fig. 15 Plot of deceleration parameter (q) versus redshift (z)

9 Deceleration parameter

The evolution of the cosmos can be described by the deceleration parameter (q). Based on the deceleration parameter, we can test whether our model is accelerating or decelerating. It is defined as

$$q = \frac{-a\ddot{a}}{\dot{a}^2} \tag{48}$$

here, a is the scale factor, if $q > 0$, the model decelerates; if $-1 < q < 0$, the model accelerates, if $q = 0$ a stable rate in expansion will be observed. Further, if $q = -1$, the universe shows de Sitter or exponential expansion; if $q < -1$, the universe shows super exponential expansion. The value of q for our model is obtained as

$$q = -\frac{exp(-\gamma_1 t)(c_1 exp(\gamma_1 t) + 3c_2 \gamma_1)}{c_1} \tag{49}$$

According to observations from high redshift supernova, type Ia supernova combined with BAO and CMB observations investigated that present-day universe is undergoing a phase of transition from deceleration to acceleration.

The plot of deceleration parameter (q) with respect to redshift (z) for $c_1 = 0.265$, $c_2 = -1.25$, $\gamma_1 = 0.12$ is shown in Fig. 15. It is observed that in the present model, the transition of universe occurs at $z_t = 0.6$ for $q = 0$. This $z_t = 0.6$ matches with observations obtained by various theoretical values by Busca [103] $z_t = 0.82 \pm 0.08$, Capozziello et al. [104], $z_t = 0.7679^{+0.1831}_{-0.1829}$, Yang and Gong [105] $z_t = 0.60^{+0.21}_{-0.12}$, Lu et al. [106] $z_t = 0.69^{+0.23}_{-0.12}$. In the present model, the decelerating phase is observed for $q > 0$, accelerating phase is observed for $q < 0$. The present value of the deceleration parameter is obtained as $q = -0.6758$.

10 Stability analysis

In this section, the stability analysis of Tsallis, Renyi and Sharma–Mittal HDE models is verified through an important quantity namely squared speed of sound (v_s^2). The value of v_s^2 is identified as

$$v_s^2 = \frac{\dot{p}_{de}}{\dot{\rho}_{de}} = \omega_{de} + \frac{\rho_{de}}{\dot{\rho}_{de}} \dot{\omega}_{de} \tag{50}$$

Fig. 16 Plot of squared speed of sound (v_s^2) of THDE versus redshift (z)
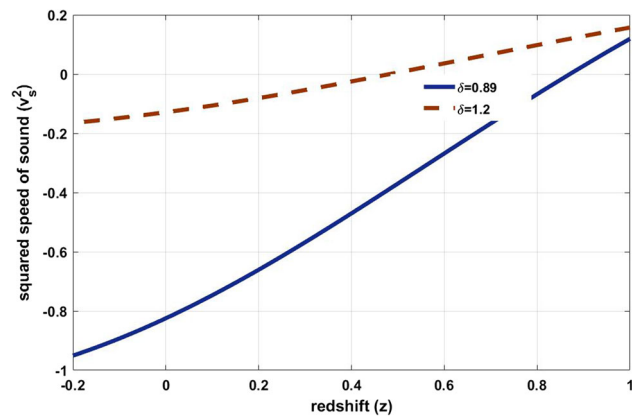
Fig. 17 Plot of squared speed of sound (v_s^2) of RHDE versus redshift (z)
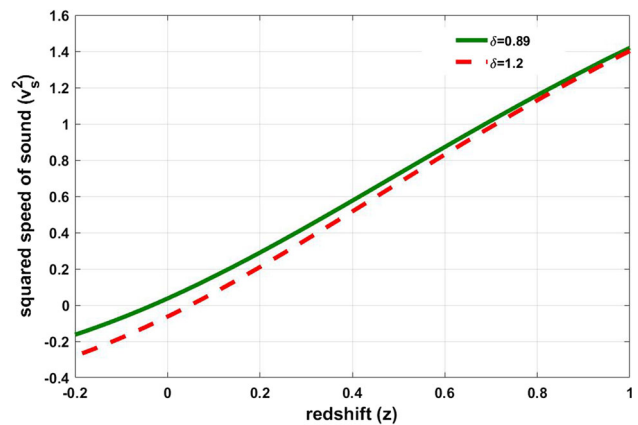
Fig. 18 Plot of squared speed of sound (v_s^2) of SHDE versus redshift (z)
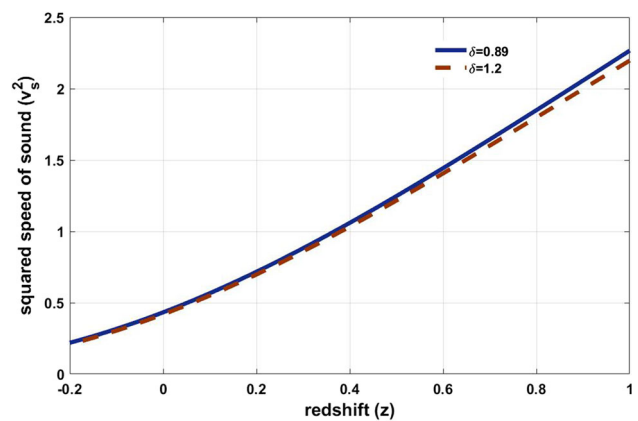
The stability of the model is described depending on the signature of v_s^2. The model is said to be stable if v_s^2 is positive, whereas it is unstable if v_s^2 is negative. The squared speed of sound v_s^2 value for the three models is given in the appendix section.

The behavior of v_s^2 for all the three models corresponding to redshift (z) is shown in Figs. 16, 17, 18, respectively. For both the values of $\delta = 0.89$, 1.2 in Tsallis HDE model the $v_s^2 < 0$ which indicates unstable behavior of the model, whereas in Renyi HDE model for $\delta = 0.89$ it is observed that $v_s^2 > 0$ in early-times and at present ($z = 0$) which indicates stable behavior of the model, $v_s^2 < 0$ for late-times which indicates unstability. For $\delta = 1.2$ in Renyi HDE $v_s^2 > 0$ in early-times indicating stable behavior of model, $v_s^2 < 0$ at present ($z - 0$), late-times indicating unstable behavior model of the universe. Sharma–Mittal HDE model exhibits stable behavior throughout for both the values of $\delta = 0.89$, 1.2 as $v_s^2 > 0$.

Fig. 19 Plot of r versus s
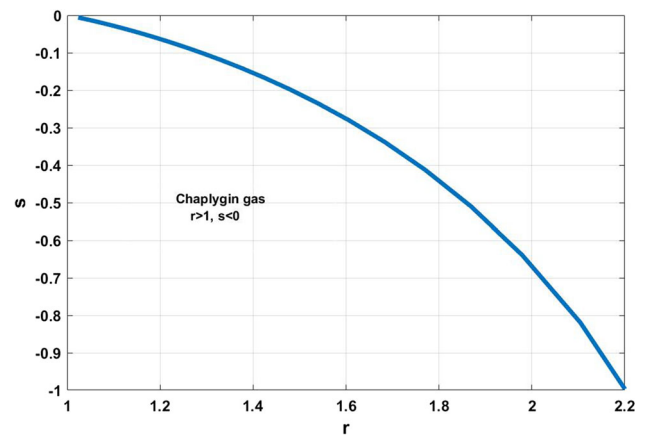
11 Statefinder parameters

The expansion of the present-day cosmos in an accelerating way is being illustrated by much dark energy (DE) models. Many dark energy models have been constructed to overcome the fine-tuning issue and analyze the cosmos accelerating phase. A cosmological diagnostic pair (r, s) known as statefinder parameter to discuss these various forms of dark energy models was proposed by Shani et al. [107], Alam et al. [108]which is defined as

$$r = \frac{\dddot{a} a^2}{\dot{a}^3} \quad , \quad s = \frac{r-1}{3\left(q - \frac{1}{2}\right)} \tag{51}$$

here, q is the deceleration parameter, a is the scale factor, and H is the Hubble parameter. The study of dark energy in (r, s) parameter is being independent of the model, instead of depending on the theory of gravity. Hence, the statefinder is referred to as a 'geometric' tool as it depends on the scale and the metric describing space-time. This geometric tool is analyzed for various dark energy candidates, including holographic dark energy, agegraphic dark energy, quintessence, Chaplygin gas, etc. The values of these parameters obtained for our model are as follows

$$r = \frac{(exp(2\gamma_1 t)c_1^2 + 9c_2^2\gamma_1^2)exp(-2\gamma_1 t)}{c_1^2} \tag{52}$$

$$s = -\frac{2c_2^2\gamma_1^2(c_2^3\gamma_1^3 exp(-\gamma_1 t) + c_1^3 exp(2\gamma_1 t) + 3\gamma_1 c_1^2 c_2 exp(\gamma_1 t) + 3\gamma_1^2 c_1 c_2^2)}{c_1(c_1 exp(\gamma_1 t) + c_2\gamma_1)^3(c_1 exp(\gamma_1 t) + 2c_2\gamma_1)} \tag{53}$$

The graphical representation of statefider parameter (r, s) is shown in Fig. 19. For all values of r, we have $s < 0$ which indicates the present model is exhibiting Chaplygin gas and at late-times it reaches to ΛCDM model $(r = 1, s = 0)$.

12 Analysis of solution through perturbation techniques

The solutions of the present model are verified through perturbation technique. This process is carried by many researchers like, Chen and Kao [109] who have studied the perturbations in anisotropic space-time in a detailed manner, in $f(R, T)$ theory this analysis is done by Sharif and Zubair [110]. Sahoo et al. [111], Saha et al. [112], Sharma et al. [113], have studied perturbation techniques in both isotropic and anisotropic models for obtaining desired results. For the three expansion factors a_i the perturbations of metric are given as

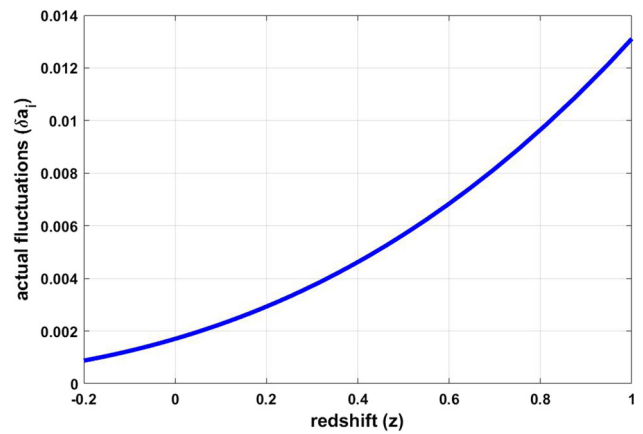$$a_i \to a_{B_i} + \delta a_i = a_{B_i}(1 + \delta b_i) \tag{54}$$

Corresponding to the above equation the perturbations expression in terms of volume $(V_B = \Pi_{i=1}^3 a_i)$, directional Hubble parameter $(\theta_i = \frac{\dot{a}_i}{a})$, mean Hubble parameter $(\theta = \sum_{i=1}^3 \frac{\theta_i}{3})$ is given as

$$V \to V_B + V_B \sum_i \delta b_i$$

$$\theta_i \to \theta_{B_i} + \sum_i \delta b_i$$

Fig. 20 Plot of actual fluctuations (δa_i) versus redshift (z)

$$\theta \to \theta_B + \frac{1}{3} \sum_i \delta b_i$$

The linear order perturbations δb_i of the metric perturbations satisfy the following conditions

$$\sum_i \delta \ddot{b}_i + 2 \sum \theta_{B_i} \delta \dot{b}_i = 0 \tag{55}$$

$$\delta \ddot{b}_i + \frac{\dot{V}_B}{V_B} \delta \dot{b}_i + \sum \delta \dot{b}_j \theta_{B_i} = 0 \tag{56}$$

$$\sum \delta \dot{b}_i = 0 \tag{57}$$

By solving these three equations (55)-(57), we obtain

$$\delta \ddot{b}_i + \frac{\dot{V}_B}{V_B} \delta \dot{b}_i = 0 \tag{58}$$

Here, in equation (58) V_B is volume, for present model V_B is given as

$$V_B = \frac{(2l+1)(c_1 exp(\gamma_1 t) + c_2 \gamma 1)}{\gamma_1} \tag{59}$$

with the help of equation (59) in (58) and on integrating, we obtain

$$\delta b_i = \frac{d_1(\gamma_1 t - ln(c_1 exp(\gamma_1 t) + c_2 \gamma_1))}{c_2 \gamma_1 (2l+1)} + d_2 \tag{60}$$

where d_1, d_2 are integrating constants. By substituting equation (60) in (54) we obtain the actual fluctuations $\delta a_i = a_{B_i} \delta b_i$ as

$$\delta a_i = \frac{\gamma_1}{(2l+1)(c_1 exp(\gamma_1 t) + c_2 \gamma_1)} \left(\frac{d_1(\gamma_1 t - ln(c_1 exp(\gamma_1 t) + c_2 \gamma_1))}{c_2 \gamma_1 (2l+1)} + d_2 \right) \tag{61}$$

Figure 20 shows that the actual fluctuations (δa_i) are plotted against redshift (z). The δa_i initially starts with small positive value and later approaches to zero value, which indicates the background solution is stable corresponding to perturbations of gravitational field.

13 Conclusions

The scalar fields in the universe produce long-range forces. Due to this reason, the scalar-tensor theories are fundamental in various disciplines in cosmology and gravitational physics. The dark matter or missing matter issue in cosmology is not discussed in Einstein's general theory of relativity. But an alternative to Einstein's theory, scalar-tensor theories can discuss these problems. These dimensionless scalar field models have been studied by several authors. Due to these interesting aspects in the present work, we have worked with the Saez–Ballester scalar-tensor theory of gravitation. Here, we studied the homogeneous and anisotropic axially symmetric metric. The field equations of this space-time are obtained using Saez–Ballester theory by considering the two fluids, one being pressureless matter and the second being HDE (Tsallis, Renyi, Sharma–Mittal models). Moreover, in the study of these three Tsallis, Renyi, Sharma–Mittal HDE models, we constructed different cosmological parameters along with their graphical

representation such as deceleration parameter, EoS parameter, squared speed of sound (v_s^2), statefinder parameters (r, s) for two different values of $\delta = 0.89$, 1.2 and observed the following.

∗ The graphical behavior of scalar field (ϕ) with respect to redshift (z) is shown in Fig. 1 and it is observed that scalar field (ϕ) is positive throughout the evolution of cosmos and it increases as redshift (z) decreases. From the behavior of this plot along with the plots of matter energy density, energy density of Tsallis HDE, Renyi HDE, and Sharma–Mittal HDE, it is observed that there is a clear contribution from the scalar field and the HDE to the cosmic expansion. Because as the scalar field increases, the dominance of matter energy density ρ_m, the energy density ρ_{de} of Tsallis, Renyi, Sharma–Mittal HDE is delayed considerably and both the energy densities were positive throughout the evolution of cosmos and decreases as redshift (z) decreases, which shows the expansion of cosmos.

∗ For the obtained three models, the energy density (ρ_m) of pressureless matter and energy density (ρ_{de}) of Tsallis, Renyi, Sharma–Mittal HDE models are positive throughout the evolution of cosmos and decreases as redshift (z) decreases for both values of $\delta = 0.89$, 1.2 which is shown in Figs. 2, 3, 5, 6 and 8, 9.

∗ The skewness parameters (γ) for all the three Tsallis, Renyi, Sharma–Mittal HDE models are positive throughout the evolution of cosmos and increases as redshift (z) decreases. In Figs. 4, 7 and 10, the behavior of the skewness parameter with respect to redshift (z) is plotted.

∗ From Fig. 11, it is observed that volume is positive throughout the evolution of cosmos and increases as redshift (z) decreases this indicates that the present universe is expanding in an accelerating way.

∗ The deceleration parameter (q) in the present work shows the transition from decelerating phase to the accelerating phase, which agrees with recent observational data. The transition (z_t) observed is $z_t = 0.6$, and the present value of the deceleration parameter is $q = -0.6758$, and it is in the acceptable range.

∗ In modern cosmology, the EoS parameter plays an important role as it controls the gravitational properties of DE and its evolution. The EoS parameter (ω_{de}) of Tsallis HDE model for $\delta = 0.89$ exhibits phantom behavior ($\omega_{de} < -1$), and for $\delta = 1.2$ it exhibits quintom like behavior (i.e., ω_{de} starts from quintessence phase, passes through phantom divide line ($\omega_{de} = -1$) and reaches the phantom phase) which represents the accelerating expansion of universe.

∗ In the case of the RHDE model, the EoS parameter (ω_{de}) for the values of $\delta = 0.89$, 1.2 shows the transition from decelerating phase to accelerating phase at $z = 0.67$, 0.72, respectively, and the model starts from matter-dominated phase exhibiting quintom like behavior. In Sharma–Mittal HDE, the EoS parameter for the values of $\delta = 0.89$, 1.2 shows the transition from decelerating phase to accelerating phase at $z = 0.475$. It enters into the quintessence phase from the matter-dominated phase, representing the universe's accelerating expansion. The EoS parameter ω_{de} for the three HDE models in the present work meets the range $\omega_{de} = -1.13^{+0.24}_{-0.25}$ [114](Planck+nine years WMAP), SNe Ia data with galaxy clustering, CMBR anisotropy statistics $-1.33 < \omega_{de} < -0.79$ and $-1.67 < \omega_{de} < -0.62$ [115], respectively, and present Planck collaboration data (2018) [116] gives the range of EoS as $\omega_{de} = -1.028 \pm 0.031$ (68%, Planck TT, TE, EE+lowE+ lensing+SNe+BAO), $\omega_{de} = -0.76 \pm 0.20$ (Planck+BAO/RSD+WL), $\omega_{de} = -0.957 \pm 0.080$ (Planck+SNe+BAO), $\omega_{de} < -0.95$ (95%, Planck TT, TE, EE+low E+ lensing+SNe+BAO) with these observations the EoS parameter (ω_{de}) in present model matches with recent observational data. The complete behavior of EoS parameters for three models is plotted in Figs. 12, 13 and 14.

∗ The stability analysis of these three HDE models is verified through squared speed of sound (v_s^2) and depicted in Figs. 16, 17, 18. The Tsallis HDE model shows unstable behavior for both the $\delta = 0.89$, 1.2. The Renyi HDE model shows stable behavior at present and early times for $\delta = 0.89$, and at late times it shows unstable behavior. Whereas for $\delta = 1.2$ it exhibits stability at early times, unstability at present, and late times. The v_s^2 of Sharma–Mittal is always positive, so it shows stable behavior throughout the universe's expansion for both the values of $\delta = 0.89$, 1.2.

∗ Statefinder parameters are plotted in Fig. 19 and observed that initially, it represents Chaplygin gas model ($r > 1$, $s < 0$) and later approaches to ΛCDM model. The background solutions for the obtained models are verified through perturbation techniques and observed that background solutions are stable against perturbation of the gravitational field represented in Fig. 20.

Finally, Tsallis, Renyi, Sharma–Mittal HDE models are obtained, and different cosmological parameters like deceleration parameter, EoS parameter, squared speed of sound, statefinder parameters, etc., are discussed thoroughly. The value of $q = -0.6758$ obtained in this work matches with recent observational data. Interestingly, all the obtained values match the recent observational data, and this type of study can be extended to other anisotropic models.

Data Availability Statement Data sharing is not applicable to this article as no datasets were generated or analyzed during the current study.

Declarations

Conflict of interest The authors declare that they have no competing interests.

Appendix

$$\iota_3 = \frac{216\pi(-1+l)exp(-3\gamma_1 t)(c_1 exp(\gamma_1 t)+c_2\gamma_1)\left(c_1^2 exp(2\gamma_1 t)(\delta\pi+\frac{\gamma_1^2}{9})+2\gamma_1 c_2\pi\delta\left(c_1 exp(\gamma_1 t)+\frac{c_2\gamma_1}{2}\right)\right)}{c^2\gamma_1^2 c_1^3(2l+1)^2}$$

$$\iota_4 = \frac{4\gamma_1 c_2 exp(-\gamma_1 t)\left(c_1^2 exp(2\gamma_1 t)\left(\delta\pi+\frac{\gamma_1^2}{18}\right)+2\gamma_1 c_2\pi\delta\left(c_1 exp(\gamma_1 t)+\frac{c_2\gamma_1}{2}\right)\right)}{c_1\left(c_1^2 exp(2\gamma_1 t)\left(\delta\pi+\frac{\gamma_1^2}{9}\right)+2\gamma_1 c_2\pi\delta\left(c_1 exp(\gamma_1 t)+\frac{c_2\gamma_1}{2}\right)\right)}$$

$$\iota_5 = -\frac{216\pi R(-1+l)exp(-3\gamma_1 t)\left(c_1 exp(\gamma_1 t)+c_2\gamma_1\right)^3}{c^2\gamma_1^2 c_1^3(2l+1)^2(\iota_7-1)}$$

$$\iota_6 = -\frac{1}{(\iota_7-1)c_1\left(c_1^2 exp(2\gamma_1 t)\left(\delta\pi+\frac{\gamma_1^2}{9}\right)+2\gamma_1 c_2\pi\delta\left(c_1 exp(\gamma_1 t)+\frac{c_2\gamma_1}{2}\right)\right)}$$

$$2\gamma_1 c_2\left(\left(\pi c_2^2\gamma_1^2(R-2\delta)exp(-\gamma_1 t)+c_1\left(c_1 exp(\gamma_1 t)\left(\frac{-2\gamma_1^2}{9}+\pi(R-2\delta)\right)+2\pi\gamma_1 c_2(R-2\delta)\right)\right)\iota_7\right.$$

$$\left.+2\pi c_2^2\delta\gamma_1^2 exp(-\gamma_1 t)+2c_1\left(c_1 exp(\gamma_1 t)\left(\delta\pi+\frac{\gamma_1^2}{9}\right)+2\gamma_1 c_2\pi\delta\right)\right)$$

$$\iota_7 = \left(\frac{(9\pi exp(2\gamma_1 t)c_1^2\delta+18\pi exp(\gamma_1 t)c_1 c_2\delta\gamma_1+9\pi c_2^2\delta\gamma_1^2+c_1^2 exp(2\gamma_1 t)\gamma_1^2)exp(-2\gamma_1 t)}{c_1^2\gamma_1^2}\right)^{R/\delta}$$

By using Eqs. (32), (37), (42), (45), (46), (47) and its derivatives in (50), we obtain the expressions for v_s^2. The following equations (62), (63), (64) represent v_s^2 for Tsallis, Renyi, Sharma–Mittal HDE models, respectively. These are as follows

$$v_s^2 = \frac{2\exp(-\gamma_1 t)}{\alpha c_1^3\gamma_1^2(-2+\delta)\left(l+\frac{1}{2}\right)^2}\left(\frac{-819^{-\delta}(-1+l)\exp(-2\gamma_1 t)(c_1\exp(\gamma_1 t)+c_2\gamma_1)^3(3H)^{2\delta}}{16}\right.$$
$$\left.+\alpha c_1^2\gamma_1^3 c_2(-2+\delta)\left(\delta-32\left(l+\frac{1}{2}\right)^2\right)\right) \tag{62}$$

$$v_s^2 = \frac{\iota_8}{\iota_9} \tag{63}$$

$$v_s^2 = \frac{1}{\iota_{10}}\iota_{11} \tag{64}$$

where

$$\iota_8 = -3exp(-3\gamma_1 t)\left(\gamma_1 c_1^6\left(\gamma_1^6\left(\left(\pi\left(\frac{1}{162}-\frac{l}{162}\right)+\frac{c^2(l+\frac{1}{2})^2}{486}\right)+\frac{\delta\pi\gamma_1^4\left(\pi(-9l+9)+c^2(l+\frac{1}{2})^2\right)}{18}\right.\right.\right.$$

$$+\delta^2\pi^2\gamma_1^2\left(\left(\frac{15}{2}-\frac{15l}{2}\right)\pi+c^2\left(l+\frac{1}{2}^2\right)\right)-\frac{63\pi^4\delta^3(-1+l)}{2}\right)c_2 exp(6\gamma_1 t)+\left(6\gamma_1^3 c_1^4\left(\left(\pi\left(-\frac{l}{36}+\frac{1}{36}\right)\right.\right.\right.$$

$$+\frac{c^2(l+\frac{1}{2})^2}{108}\right)\gamma_1^4+\delta\pi\gamma_1^2\left(\pi\left(\frac{-5l}{2}+\frac{5}{2}\right)+c^2\left(l+\frac{1}{2}\right)^2\right)-\frac{105\pi^3\delta^2(-1+l)}{4}\right)\delta c_2^3 exp(4\gamma_1 t)$$

$$+4\gamma_1^2\left(\left(\pi\left(-\frac{l}{8}+\frac{1}{8}\right)+\frac{c^2(l+\frac{1}{2})^2}{36}\right)\gamma_1^4+\delta\pi\gamma_1^2\left(\pi\left(-\frac{15l}{4}+\frac{15}{4}\right)+c^2\left(l+\frac{1}{2}\right)^2\right)-\frac{189\pi^3\delta^2(-1+l)}{8}\right)\right)$$

$$c_1^5\delta c_2^2 exp(5\gamma_1 t)+\gamma_1^5 c_1^2\left(\left(\pi\left(\frac{3}{2}-\frac{3l}{2}\right)+c^2(l+1/2)^2\right)\gamma_1^2-\frac{189\delta\pi^2(-1+l)}{2}\right)\delta^2\pi c_2^5 exp(2\gamma_1 t)$$

$$-\frac{9\left(\delta\pi+\frac{\gamma_1^2}{9}\right)^3 c_1^7(-1+l)exp(7\gamma_1 t)}{2}+4\gamma_1^4\delta^2\pi c_2^4\left(c_1^3\left(\left(\pi\left(\frac{-15l}{8}+\frac{15}{8}\right)+c^2\left(l+\frac{1}{2}\right)^2\right)\gamma_1^2\right.\right.$$

$$-\frac{315\delta\pi^2(-1+l)}{8}\Big)exp(3\gamma_1 t)-\frac{63\gamma_1^2\big(c_1 exp(\gamma_1 t)+\frac{c_2\gamma_1}{7}\big)(-1+l)\delta\pi^2 c_2^2}{8}\Big)\Big)\pi\Big)$$

$$\iota_9=\gamma_1^2 c^2 c_1^3\Big(l+\frac{1}{2}\Big)^2\Big(c_1^2 exp(2\gamma_1 t)\Big(\delta\pi+\frac{\gamma_1^2}{9}\Big)+2\gamma_1\delta\pi c_2\big(c_1 exp(\gamma_1 t)+\frac{c_2\gamma_1}{2}\big)\Big)\Big(c_1^2\Big(\delta\pi+\frac{\gamma_1^2}{18}\Big)exp(2\gamma_1 t)$$

$$+2\gamma_1\big(c_1 exp(\gamma_1 t)+\frac{c_2\gamma_1}{2}\big)\delta\pi c_2\Big)$$

$$\iota_{10}=2c^2\Bigg(\frac{c_1^2\big(\delta\pi+\frac{\gamma_1^2}{9}\big)exp(2\gamma_1 t)}{2}+\gamma_1(c_1 exp(\gamma_1 t)+\frac{c_2\gamma_1}{2})\delta\pi c_2\Bigg)\Big(l+\frac{1}{2}\Big)^2\gamma_1^2\Bigg(\frac{c_1^2\big(\frac{-2\gamma_1^2}{9}+\pi(R-2\delta)\big)exp(2\gamma_1 t)}{2}$$

$$+\pi\gamma_1\big(c_1 exp(\gamma_1 t)+\frac{c_2\gamma_1}{2}\big)(R-2\delta)c_2\Big)\iota_7+c_1^2\Big(\delta\pi+\frac{\gamma_1^2}{9}\Big)exp(2\gamma_1 t)+2\gamma_1\big(c_1 exp(\gamma_1 t)+\frac{c_2\gamma_1}{2}\big)\delta\pi c_2\Bigg)$$

$$\iota_{11}=-\Bigg(\Bigg(-\Big(c_1^4 exp(6\gamma_1 t)\Big(\frac{\gamma_1^4}{27}-\frac{5\pi\big(R-\frac{12\delta}{5}\big)\gamma_1^2}{18}+\pi^2(R-2\delta)\Big(R-\frac{3\delta}{2}\Big)\Big)+\pi\Big(6\Big(\gamma_1^2\Big(\frac{-5R}{108}+\frac{\delta}{9}\Big)$$

$$+\pi\Big(R-\frac{3\delta}{2}\Big)(R-2\delta)\Big)\gamma_1 c_2 c_1^2 exp(4\gamma_1 t)+4\Big(\gamma_1^2\Big(\frac{-5R}{36}+\frac{\delta}{3}\Big)+\pi(R-2\delta)\Big(R-\frac{3\delta}{2}\Big)\Big)c_1^3 exp(5\gamma_1 t)$$

$$+\Big(R-\frac{3\delta}{2}\Big)\pi(exp(2\gamma_1 t)c_2\gamma_1+4c_1 exp(3\gamma_1 t))\gamma_1^2(R-2\delta)c_2^2\Big)\gamma_1 c_2\Big)c^2\Big(l+\frac{1}{2}\Big)^2\gamma_1^3 c_2 c_1^2\iota_7$$

$$+\Bigg(\gamma_1 c_2 c_1^6 exp(6\gamma_1 t)\Bigg(\frac{2c^2\gamma_1^6\big(l+\frac{1}{2}\big)^2}{27}-\frac{5\pi\gamma_1^4\Big(\frac{-24\delta\big(l+\frac{1}{2}\big)^2 c^2}{5}+R\big(c^2\big(l+\frac{1}{2}\big)^2-\frac{9l}{5}+\frac{9}{5}\big)\Big)}{18}$$

$$+\pi^2\Big(6c^2\Big(l+\frac{1}{2}\Big)^2\delta^2-\frac{7R\big(c^2\big(l+\frac{1}{2}\big)^2-\frac{30l}{7}+\frac{30}{7}\big)\delta}{2}+R^2 c^2\Big(l+\frac{1}{2}\Big)^2\Big)\gamma_1^2+\frac{189\pi^3 R\delta^2(-1+l)}{2}\Bigg)$$

$$+\Bigg(6\gamma_1^3 c_2^3\Big(\gamma_1^4\Big(\frac{2\delta\big(l+\frac{1}{2}\big)^2 c^2}{9}-\frac{5R\big(c^2\big(l+\frac{1}{2}\big)^2-\frac{3l}{5}+\frac{3}{5}\big)}{108}\Big)+\Big(6c^2\Big(l+\frac{1}{2}\Big)^2\delta^2$$

$$-\frac{7R\delta\big(c^2\big(l+\frac{1}{2}\big)^2-\frac{10l}{7}+\frac{10}{7}\big)}{2}+R^2 c^2\Big(l+\frac{1}{2}\Big)^2\Big)\pi\gamma_1^2+\frac{315\pi^2 R\delta^2(-1+l)}{4}\Big)c_1^4 exp(4\gamma_1 t)$$

$$+4\Big(\gamma_1^4\Big(\frac{2\delta\big(l+\frac{1}{2}\big)^2 c^2}{3}-\frac{5R\big(c^2(l+1/2)^2-\frac{9l}{10}+\frac{9}{10}\big)}{36}\Big)+\pi\Big(6c^2\Big(l+\frac{1}{2}\Big)^2\delta^2$$

$$-\frac{7R\big(c^2\big(l+\frac{1}{2}\big)^2-\frac{15l}{7}+\frac{15}{7}\big)\delta}{2}+R^2 c^2\Big(l+\frac{1}{2}\Big)^2\Big)\gamma_1^2+\frac{567\pi^2 R\delta^2(-1+l)}{8}\Big)\gamma_1^2 c_2^2 c_1^5 exp(5\gamma_1 t)$$

$$+\Bigg(\Big(\Big(6c^2\Big(l+\frac{1}{2}\Big)^2\delta^2-\frac{7\big(c^2\big(l+\frac{1}{2}\big)^2-\frac{6l}{7}+\frac{6}{7}\big)R\delta}{2}+R^2 c^2\Big(l+\frac{1}{2}\Big)^2\Big)\gamma_1^2+\frac{567\pi R\delta^2(-1+l)}{2}\Big)\pi\gamma_1^5 c_2^5 c_1^2$$

$$exp(2\gamma_1 t)+4\pi\gamma_1^4 c_2^4 c_1^3 exp(3\gamma_1 t)\gamma_1^2\Big(6c^2\Big(l+\frac{1}{2}\Big)^2\delta^2-\frac{7R\big(c^2\big(l+\frac{1}{2}\big)^2-\frac{15l}{14}+\frac{15}{14}\big)\delta}{2}+R^2 c^2\Big(l+\frac{1}{2}\Big)^2\Big)$$

$$+\frac{945\pi R\delta^2(-1+l)}{8}\Bigg)+\frac{189(-1+l)R\left(\frac{\left(\delta\pi+\frac{\gamma_1^2}{9}\right)^2 c_1^7 exp(7\gamma_1 t)}{7}+\pi^2 c_2^6\delta^2\gamma_1^6\left(c_1 exp\gamma_1 t+\frac{c_2\gamma_1}{7}\right)\right)}{2}\Bigg)\Bigg)\pi\Bigg)\iota_7$$

$$-\frac{1}{2}\Bigg(189\gamma_1\left(\delta\pi+\frac{\gamma_1^2}{9}\right)c_2 c_1^6 exp(6\gamma_1 t)\left(\frac{(2c^2(l+\frac{1}{2})^2\gamma_1^4)}{567}+\frac{\pi\gamma_1^2\left(\frac{2\delta\left(l+\frac{1}{2}\right)^2 c^2}{3}+R(-1+l)\right)}{21}+\pi^2 R\delta(-1+l)\right)\Bigg)$$

$$-\frac{1}{2}189\pi\Bigg(5\Bigg(\gamma_1^4\left(\frac{4\delta\left(l+\frac{1}{2}\right)^2 c^2}{2835}+\frac{R(-1+l)}{2835}\right)+\frac{4\delta\left(\frac{3\delta\left(l+\frac{1}{2}\right)^2 c^2}{5}+R(-1+l)\right)\pi\gamma_1^2}{63}+\pi^2 R\delta^2$$

$$(-1+l))\gamma_1^3 c_2^3 c_1^4 exp(4\gamma_1 t)+3\gamma_1^2 c_2^2 c_1^5 exp(5\gamma_1 t)\left(\gamma_1^4\left(\frac{8\delta\left(l+\frac{1}{2}\right)^2 c^2}{1701}+\frac{R(-1+l)}{567}\right)\right.$$

$$+\frac{20\delta\pi\left(\frac{2\delta\left(l+\frac{1}{2}\right)^2 c^2}{5}+R(-1+l)\right)\gamma_1^2}{189}+\pi^2 R\delta^2(-1+l)\Bigg)+3\delta\pi\gamma_1^5 c_2^5 c_1^2 exp(2\gamma_1 t)$$

$$\left(\gamma_1^2\left(\frac{2\delta\left(l+\frac{1}{2}\right)^2 c^2}{189}+\frac{2R(-1+l)}{189}\right)+\pi R\delta(-1+l)\right)+5\delta\pi\gamma_1^4 c_2^4 c_1^3$$

$$\left(\gamma_1^2\left(\frac{8\delta\left(l+\frac{1}{2}\right)^2 c^2}{315}+\frac{2R(-1+l)}{63}\right)+\pi R\delta(-1+l)\right)exp(3\gamma_1 t)+(-1+l)R$$

$$\frac{\left(\delta\pi+\frac{\gamma_1^2}{9}\right)^2 c_1^7 exp(7\gamma_1 t)}{7}+\pi^2 c_2^6\delta^2\gamma_1^6\left(c_1 exp(\gamma_1 t)+\frac{c_2\gamma_1}{7}\right)\Bigg)\Bigg)\Bigg)\Bigg)\Bigg)exp(-3\gamma_1 t)$$

References

1. A.G. Riess et al., Observational evidence from supernovae for an accelerating Universe and a cosmological constant. Astron. J. **116**, 1009–1038 (1998)
2. S. Perlmutter et al., Measurements of Ω and Λ from 42 high-redshift supernovae. Astrophys. J. **517**, 565–586 (1999)
3. P. Bernardis et al., A flat Universe from high-resolution maps of the cosmic microwave background radiation. Nature **404**, 955–959 (2000)
4. S. Perlmutter et al., New constraints on and w from an independent set of 11 high-redshift supernovae observed with the hubble space telescope. Astrophys. J. **598**, 102–137 (2003)
5. S. Hanany et al., MAXIMA-1: A measurement of the cosmic microwave background anisotropy on angular scales of 10 arcminutes to 5 degrees. Astrophys. J. Lett. **545**, L5–L9 (2000)
6. C.B. Netterfield et al., A measurement by BOOMERANG of multiple peaks in the angular power spectrum of the cosmic microwave background. Astrophys. J. **571**, 604–614 (2002)
7. D.N. Spergel et al., First year wilkinson microwave anisotropy probe (WMAP) observations: determination of cosmological parameters. Astrophys. J. Suppl. **148**, 175–194 (2003)
8. M. Colless et al., The 2dF galaxy redshift survey: spectra and redshift. Mon. Not. R. Astron. Soc. **328**, 1039–1063 (2001)
9. M. Tegmark et al., Cosmological parameters from SDSS and WMAP. Phys. Rev. D **69**, 103501–103526 (2004)
10. S. Cole et al., The 2dF galaxy redshift survey: Power-spectrum analysis of the final dataset and cosmological implications. Mon. Not. R. Astron. Soc. **362**, 505–534 (2005)
11. V. Springel, C.S. Frenk, S.M.D. White, The large-scale structure of the universe. Nature **440**, 1137–1144 (2006)
12. C.H. Brans, R.H. Dicke, Mach's principle and a relativistic theory of gravitation. Phys. Rev. D **124**, 925–935 (1961)
13. D. Saez, V.J. Ballester, A simple coupling with cosmological implications. Phys. Lett. A **113**, 467–470 (1986)
14. A.D. Felice, S. Tsujikawa, $f(R)$ Theories. Living Rev. Relativ. **13**, 3–163 (2010)
15. V. Sahni, The cosmological constant problem and quintessence. Class. Quant. Grav. **19**, 3435–3448 (2002)

16. S. Nojiri, S.D. Odintsov, Unified cosmic history in modified gravity: from $f(R)$ theory to Lorentz non-invariant models. Phys. Rep. **505**, 59–144 (2011)
17. E.V. Linder, Einstein's other gravity and the acceleration of the universe. Phys. Rev. D **81**, 127301–127303 (2010)
18. R. Ferraro, F. Fiorini, Non-trivial frames for $f(T)$ theories of gravity and beyond. Phys. Lett. B **702**, 75–80 (2011)
19. M. Sharif, S. Rani, Wormhole solutions in $f(T)$ gravity with noncommutative geometry. Phys. Rev. D **88**, 123501–123510 (2013)
20. T. Harko, S.N. Francisco, F.S.N. Lobo, S. Nojiri, S.D. Odintsov, $f(R, T)$ gravity. Phys. Rev. D **84**, 024020–024031 (2011)
21. S. Weinberg, The cosmological constant problem. Rev. Mod. Phys. **61**, 1 (1989)
22. J. Martin, The phenomenological approach to modeling the dark energy. Compt. Rend. Phys. **13**, 566 (2012)
23. M. Malekjani, T. Naderi, F. Pace, Effects of ghost dark energy perturbations on the evolution of spherical overdensities. Mon. Not. R. Astron. Soc B **453**, 4148–4158 (2015)
24. C. Armendariz-Picon, V. Mukhanov, P.J. Steinhardt, Essentials of k-essence. Phys. Rev. D **63**, 103510 (2001)
25. T. Chiba, Tracking k-essence. Phys. Rev. D **66**, 063514 (2002)
26. I. Zlatev, L. Wang, P.J. Steinhardt, Quintessence, Cosmic Coincidence, and the Cosmological Constant. Phys. Rev. Lett. 1999, **82**, 896 (1999)
27. R.R. Caldwell, M. Kamionkowski, N.N. Weinberg, Phantom energy: dark energy with $\omega < 1$ causes a cosmic doomsday. Phys. Rev. Lett. **91**, 071301 (2003)
28. P. González-Dííaz, You need not be afraid of phantom energy. Phys. Rev. D **68**, 021303 (2003)
29. L. Amendola, F. Finelli, C. Burigana, D. Carturan, WMAP and the generalized Chaplygin gas. J. Cosm. Astrop. Phys. **7**, 005 (2003)
30. M.C. Bento, O. Bertolami, A.A. Sen, Generalized Chaplygin gas, accelerated expansion, and dark-energy-matter unification. Phys. Rev. D **66**, 043507 (2002)
31. Z. Keresztes, L.A. Gergely, AYu. Kamenshchik, V. Gorini, D. Polarski, Soft singularity crossing and transformation of matter properties. Phys. Rev. D **88**, 023535 (2003)
32. M.R. Setare, The holographic dark energy in non-flat Brans-Dicke cosmology. Phys. Lett. B **644**, 99–103 (2007)
33. K. Kleidis, N.K. Spyrou, Polytropic dark matter flows illuminate dark energy and accelerated expansion. Astron. Astrographys. **576**, A23 (2015)
34. K. Kleidis, N.K. Spyrou, Dark Energy: The Shadowy Reflection of Dark Matter. Entropy **18**, 94 (2016)
35. M. Li, A Model of holographic dark energy. Phys. Lett. B **603**, 1 (2004)
36. D. Pavon, W. Zimdahl, Holographic dark energy and cosmic coincidence. Phys. Lett. B **628**, 206 (2005)
37. Q.G. Huang, M. Li, The holographic dark energy in a non-flat universe. J. Cosm. Astrop. Phys. **8**, 013 (2004)
38. Q.G. Huang, Y. Gong, Supernova Constraints on a holographic dark energy model. arXiv:astro-ph/0403590 (2004)
39. Y. Gong, Extended holographic dark energy. Phys. Rev. D **70**, 064029 (2004)
40. G. t Hooft, Dimensional reduction in quantum gravity. arXiv:gr-qc/9310026 (1993)
41. L. Susskind, The World as a Hologram. J. Math. Phys. **36**, 6377–6396 (1995)
42. A. Cohen, D. Kaplan, A. Nelson, Effective field theory, black holes, and the cosmological constant. Phys. Rev. Lett. **82**, 4971 (1999)
43. S.D.H. Hsu, Entropy bounds and dark energy. Phys. Lett. B **594**, 13 (2004)
44. L. Xu, Holographic dark energy model with Hubble horizon as an IR cut-off. J. Cosm. Astrop. Phys. **9**, 016 (2009)
45. J. Liu, Y. Gong, X. Chen, Dynamical behavior of the extended holographic dark energy with the Hubble horizon. Phys. Rev. D **81**, 083536 (2010)
46. Y. Nomura, G.N. Remmen, Area law unification and the holographic event horizon. J. High Ener. Phys. **2018**, 063 (2018)
47. H.M. Sadjadi, The particle versus the future event horizon in an interacting holographic dark energy model. J. Cosm. Astrop. Phys **2**, 026 (2007)
48. Z.P. Huang, Y.L. Wu, Holographic dark energy model characterized by the conformal-age-like length. Int. J. Mod. Phys. A **27**, 1250085 (2012)
49. Z.P. Huang, Y.L. Wu, Cosmological constraint and analysis on holographic dark energy model characterized by the conformal age-like length. Int. J. Mod. Phys. A **27**, 1250130 (2012)
50. E.K. Li, Yu. Zhang, G.J. Ling, D. Peng-Fei, Generalized holographic Ricci dark energy and generalized second law of thermodynamics in Bianchi Type I universe. Gen. Rel. Grav. **47**, 136 (2015)
51. A. Khodam-Mohammadi, A. Pasqua, M. Malekjani, I. Khomenko, M. Monshizadeh, Statefinder diagnostic of logarithmic entropy corrected holographic dark energy with Granda-Oliveros IR cut-off. Astrophys. Spa. Sci. **345**, 415 (2013)
52. Y. Sobhanbabu, M.Vijaya Santhi, Kantowski-Sachs Tsallis holographic dark energy model with sign-changeable interaction. Eur. Phys. J. C **81**, 1040 (2021)
53. M.Vijaya Santhi, Y. Sobhanbabu, Bianchi type-III Tsallis holographic dark energy model in Saez-Ballester theory of gravitation. Eur. Phys. J. C **80**, 1198 (2020)
54. S. Abe, General pseudoadditivity of composable entropy prescribed by the existence of equilibrium. Phys. Rev. E **63**, 061105 (2001)
55. H. Touchette, When is a quantity additive and when is it extensive. Physica A **305**, 84–88 (2002)
56. A. Majhi, Non-extensive statistical mechanics and black hole entropy from quantum geometry. Phys. Lett. B **775**, 32–36 (2017)
57. C. Tsallis, L.J.L. Cirto, Black hole thermodynamical entropy. Eur. Phys. J. C **73**, 2487 (2013)
58. M. Tavayef, A. Sheykhi, K. Bamba, H. Moradpour, Tsallis holographic dark energy. Phys. Lett. B. **781**, 195–200 (2018)
59. H. Moradpour, S.A. Moosavi, I.P. Morais, I.P. Lobo, I.G. Salako, A. Jawad, Thermodynamic approach to holographic dark energy and the Renyi entropy. Eur. Phys. J. C **78**, 829 (2018)
60. A.S. Jahromi, S.A. Moosavi, H. Moradpour, I.P. Morais, I.P. Lobo, I.G. Salako, A. Jawad, Generalized entropy formalism and a new holographic dark energy model. Phys. Lett. B **780**, 21–24 (2018)
61. Y. Aditya, S. Mandal, P.K. Sahoo, Observational constraint on interacting Tsallis holographic dark energy in logarithmic Brans-Dicke theory. Eur. Phys. J. C **79**, 1020 (2019)
62. U.Y. Divya Prasanthi, Y. Aditya, Anisotropic Renyi holographic dark energy models in general relativity. Results Phys. **17**, 103101 (2020)
63. U.Y. Divya Prasanthi, Y. Aditya, Observational constraints on Renyi holographic dark energy in Kantowski-Sachs universe. Phys. Dark Univ. **31**, 100782 (2021)
64. M. Younas, A. Jawad, S. Qummer, H. Moradpour, S. Rani, Cosmological implications of the generalized entropy based holographic dark energy models in dynamical chern-simons modified gravity. Adv. High Energy Phys. 1287932 (2019)
65. S. Maity, U. Debnath, Tsallis, Renyi and Sharma-Mittal holographic and new agegraphic dark energy models in D-dimensional fractal universe. Eur. Phys. J. Plus **134**, 514 (2019)
66. A. Iqbal, A. Jawad, Tsallis, Renyi and Sharma-Mittal holographic dark energy models in DGP brane-world. Phys. Dark Univ. **26**, 100349 (2019)
67. A. Jawad, K. Bamba, M. Younas, S. Qummer, S. Rani, Tsallis, Rényi and Sharma-Mittal holographic dark energy models in loop quantum cosmology. Symmetry **10**, 635 (2018)
68. C.L. Bennett et al., First-year wilkinson microwave anisotropy probe (WMAP) observations: preliminary maps and basic results. Astron. Astrophys. Suppl. Ser. **148**, 1–27 (2003)
69. O. Akarsu, C.B. Kilinc, de Sitter expansion with anisotropic fluid in Bianchi type-I space-time. Astrophys. Space Sci. **326**, 315–322 (2010)

70. G. Ramesh, S. Umadevi, LRS bianchi type-II minimally interacting holographic dark energy model in Sáez-Ballester theory of gravitation. Astrophys. Space Sci. **361**, 50 (2016)
71. V.U.M. Rao, U.Y.D. Prasanthi, Y. Aditya, Plane symmetric modified holographic Ricci dark energy model in Sáez Ballester theory of gravitation. Results Phys. **10**, 469–475 (2018)
72. S.M.M. Rasouli, P.V. Moniz, Modified Sáez-Ballester scalar-tensor theory from 5D space-time. Class. Quantum Gravity **35**, (1-23) (2018)
73. U.K. Sharma, R. Zia, A. Pradhan, Transit cosmological models with perfect fluid and heat flow in Sáez-Ballester theory of gravitation. J. Astrophys. Astron. **40**, 2 (2019)
74. C. Chawla, R.K. Mishra, A. Pradhan, A new class of accelerating cosmological models with variable G and Λ in sáez and ballester theory of gravitation. Rom. J. Phys. **59**, 12–25 (2014)
75. R.K. Mishra, H. Dua, Bulk viscous string cosmological models in Sáez-Ballester theory of gravity. Astrophys. Space Sci. **364**, 195 (2019)
76. R.K. Mishra, A. Chand, Cosmological models in Sáez-Ballester theory with bilinear varying deceleration parameter. Astrophys Space Sci. **365**, 76 (2020)
77. S.M.M. Rasouli et al., Late time cosmic acceleration in modified Saez-Ballester theory. Phys. Dark Univ. **27**, 100446 (2020)
78. V.U.M. Rao, T. Vinutha, M. Vijaya Shanthi, An exact Bianchi type-V cosmological model in Saez-Ballester theory of gravitation. Astrophys. Space Sci. **312**, 189-191 (2007)
79. C.P. Singh, M. Zeyauddin, S. Ram, Anisotropic Bianchi-V cosmological models in Saez Ballester theory of gravitation. Int. J. Modern Phys. A **28**, 2719–2731 (2008)
80. V.U.M. Rao, M. Vijaya Santhi, T. Vinutha, Exact Bianchi type II, VIII and IX string cosmological models in Saez-Ballester theory of gravitation. Astrophys. Space Sci. **314**, 73-77 (2008)
81. G.C. Samata, S.K. Biswal, P.K. Sahoo, Five Dimensional Bulk Viscous String Cosmological Models in Saez and Ballester Theory of Gravitation. Int. J. Theor. Phys. **52**, 1 (2013)
82. T. Vinutha, V.U.M. Rao, G. Bekele, M. Mengesha, Dark energy cosmological models with cosmic string. Astrophys. Space Sci. **363**, 188 (2018)
83. T. Vinutha, V.U.M. Rao, G. Bekele, K.S. Kavya, Viscous string anisotropic cosmological model in scalar-tensor theory. Indian journal of Phys. **95**, 1933 (2021)
84. M.R. Setare, The holographic dark energy in non-flat Brans-Dicke cosmology. Phys. Lett. B **644**, 99–103 (2007)
85. Narayan Banerjee, Diego Pavon, Holographic dark energy in Brans-Dicke theory. Phys. Lett. B **647**, 477–481 (2007)
86. C.P. Singh, P. Kumar, Holographic Dark Energy in Brans-Dicke Theory with Logarithmic Form of Scalar Field. Int. J. Theor. Phys. **56**, 3297–3310 (2017)
87. Dao-Jun. Liu, Hua Wang, Bin Yang, Modified holographic dark energy in DGP brane world. Phys. Lett. B **694**, 6–9 (2010)
88. M.R. Setare, E.C. Vanegas, The cosmological dynamics of interacting holographic dark energy model. Int. J. Mod. Phys. D **18**, 147 (2009)
89. Y. Aditya, D.R.K. Reddy, FRW type Kaluza-Klein modified holographic Ricci dark energy models in Brans-Dicke theory of gravitation. Eur. Phys. J. C **78**, 619 (2019)
90. S. Bhattacharaya, T.M. Karade, Uniform anisotropic cosmological model with string source. Astrophys. Space Sci. **202**, 69–75 (1993)
91. S.W. Hawking, G.F.R. Ellis, The large scale structure of Space-time, p. 88. Cambridge University Press(1975)
92. K.S. Thorne, Primordial element formation, primordial magnetic fields, and the isotropy of the universe. Astrophys. J. **148**, 51 (1967)
93. J. Kristian, R.K. Sachs, Observations in cosmology. Astrophys. J. **143**, 379 (1966)
94. R. Kantowski, R.K. Sachs, Some spatially homogeneous anisotropic relativistic cosmological models. J. Math. Phys. **7**, 433 (1966)
95. C.B. Collins, E.N. Glass, D.A. Wilkinson, Exact spatially homogeneous cosmologies. Gen. Relativ. Gravit. **12**, 805–823 (1983)
96. Y. Aditya, D.R.K. Reddy, Anisotropic new holographic dark energy model in Saez-Ballester theory of gravitation. Astrophys. Space Sci. **363**, 207 (2018)
97. B. Mishra, P.K. Sahoo, Bianchi type VI h perfect fluid cosmological model in $f(R, T)$ theory. Astrophys. Space Sci. **352**, 331–336 (2014)
98. O. Akarsu, C.B. Kilinc, LRS Bianchi type I models with anisotropic dark energy and constant deceleration parameter. Gen. Relativ. Gravit. **42**, 119–140 (2010)
99. K.S. Adhav, LRS Bianchi type-I universe with anisotropic dark energy in lyra geometry. Int. J. Astron. Astrophys. **1**, 204 (2011)
100. M. Vijaya Santhi, Y. Aditya, V.U.M. Rao, Some Bianchi type generalized ghost piligrim dark energy models in general relativity. Astrophys. Space Sci. **361**, 142 (2016)
101. M. Vijaya Santhi, V.U.M. Rao, Y. Aditya, Bianchi type-VI0 modified holographic Ricci dark energy model in a scalar-tensor theory. Can. J. Phys. **95**, 179-183 (2017)
102. B.D. Sharma, D.P. Mittal, New non-additive measures of entropy for discrete probability distributions. J. Math. Sci. **10**, 28 (1975)
103. N.G. Busca et al., Baryon acoustic oscillations in the Lyα forest of BOSS quasars. Astron. Astrophys. **552**, A96 (2013)
104. S. Capozziello, O. Farooq, O. Luongo, B. Ratra, Cosmographic bounds on the cosmological deceleration-acceleration transition redshift in $f(R)$ gravity. Phys. Rev. D **90**, 044016 (2014)
105. Y. Yang, Y. Gong, The evidence of cosmic acceleration and observational constraints. arXiv:1912.07375
106. J. Lu, L. Xu, M. Liu, Constraints on kinematic models from the latest observational data. Phys. Lett. B **699**, 246–250 (2011)
107. V. Sahni, T.D. Saini, A.A. Starobinsky, U. Alam, Statefinder-a new geometrical diagnostic of dark energy. J. Exp. T. Phys. Lett. **77**, 201–206 (2003)
108. U. Alam, V. Sahni, T.D. Saini, A.A. Starobinsky, Exploring the expanding Universe and dark energy using the statefinder diagnostic. Mon. Not. R. Astron. Soc. **344**, 1057–1074 (2003)
109. C.M. Chen, W.F. Kao, Stability analysis of anisotropic inflationary cosmology. Phys. Rev. D **64**, 124019 (2001)
110. M. Sharif, M. Zubair, Energy conditions constraints and stability of power law solutions in $f(R, T)$ gravity. J. Phys. Soc. Jpn. **82**, 014002 (2013)
111. P. Sahoo, S. Bhattacharjee, S.K. Tripathy, P.K. Sahoo, Bouncing scenario in $f(R, T)$ gravity. Phys. Lett. A **35**, 2050095 (2020)
112. B. Saha, H. Amirhashchi, P. Anirudhan, Two-fluid scenario for dark energy models in an FRW universe-revisited. Astrophys. Space Sci. **342**, 257–267 (2012)
113. L.K. Sharma, A.K. Yadav, P.K. Sahoo, B.K. Singh, Non-minimal matter-geometry coupling in Bianchi I space-time. Results Phys. **10**, 738 (2018)
114. P.A.R. Ade et al., Planck 2015 results: $XIII$ cosmological parameters. Astron. Astrophys. **594**, A13 (2016)
115. M. Tegmark et al., The three-dimensional power spectrum of galaxies from the Sloan digital sky survey. Astrophys. J. **606**, 702 (2004)
116. N. Aghanim, et al., Plancks Collaboration,Planck 2018 results. VI. Cosmological parameters. arXiv:1807.06209v2 (2018)